Journal of Polymers and the Environment (2024) 32:2797–2817
https://doi.org/10.1007/s10924-024-03261-1

ORIGINAL PAPER

Electrospun Silk Fibroin and Collagen Composite Nanofiber Incorporated with Palladium and Platinum Nanoparticles for Wound Dressing Applications

Mayakrishnan Arumugam[1] · Balaji Murugesan[2] · Dhilipkumar Chinnalagu[1] · Premkumar Balasekar[3] · Yurong Cai[2] · Ponnurengam Malliappan Sivakumar[4,5] · Gowri Rengasamy[1] · Krithikapriya Chinniah[1] · Sundrarajan Mahalingam[1]

Accepted: 23 March 2024 / Published online: 25 April 2024
© The Author(s), under exclusive licence to Springer Science+Business Media, LLC, part of Springer Nature 2024

Abstract

In the field of biomedical engineering, nanofiber scaffolds have excellent biomaterial properties, making them highly suitable for superior wound dressing applications. This work presents the fabrication of a novel bimetal blend comprising palladium and platinum nanoparticles integrated with silk fibroin and collagen composite nanofibers through the electrospinning method. The fabricated composite nanofibrous scaffolds were investigated to analyze their chemical composition, surface morphology, thermal stability, porosity, hemocompatibility, mechanical strength, swelling, and degradation properties. The average diameter length of the SF/CL/Pd–Pt composite nanofiber scaffolds is 141.62 ± 33.03 nm, with Pd and Pt nanoparticle diameters measured at 8.64 and 7.36 nm, respectively. In vitro assessments of SF/CL and SF/CL/Pd–Pt composite nanofiber scaffolds demonstrated outstanding antibacterial efficacy against both gram-positive (*S. aureus*) and gram-negative (*E. coli*) bacteria. The antioxidant activity of SF/CL/Pd–Pt composite nanofibers exhibited a free radical scavenging percentage of 94.34%. Additionally, cell proliferation studies conducted on the fibroblast (NIH3T3) cell line, along with in vivo investigations on male Sprague–Dawley rats, underscored the remarkable wound-healing ability of the SF/CL/Pd–Pt composite nanofiber scaffolds. Furthermore, histopathological examination of wounded tissue samples using H&E and Masson trichrome staining revealed faster reepithelialization, granulation, angiogenesis, and reduced inflammatory response. These findings demonstrate that SF/CL/Pd–Pt composite nanofibrous scaffolds are excellent wound dressing materials for all biomedical applications.

✉ Sundrarajan Mahalingam
drmsgreenchemistrylab@gmail.com

[1] Advanced Green Chemistry Lab, Department of Industrial Chemistry, School of Chemical Sciences, Alagappa University, Karaikudi, Tamil Nadu 630 003, India

[2] The Key Laboratory of Advanced Textile Materials and Manufacturing Technology of Ministry of Education, National Engineering Lab for Textile Fiber Materials and Processing Technology, School of Materials Science and Engineering, Zhejiang Sci-Tech University, Hangzhou 310018, China

[3] Department of Pharmacology, K.K.College of Pharmacy, Affiliated to The Tamilnadu Dr. M.G.R.Medical University, Gerugambakkam 600128, India

[4] Institute of Research and Development, Duy Tan University, Da Nang, Vietnam

[5] School of Medicine and Pharmacy, Duy Tan University, Da Nang, Vietnam

Graphical Abstract

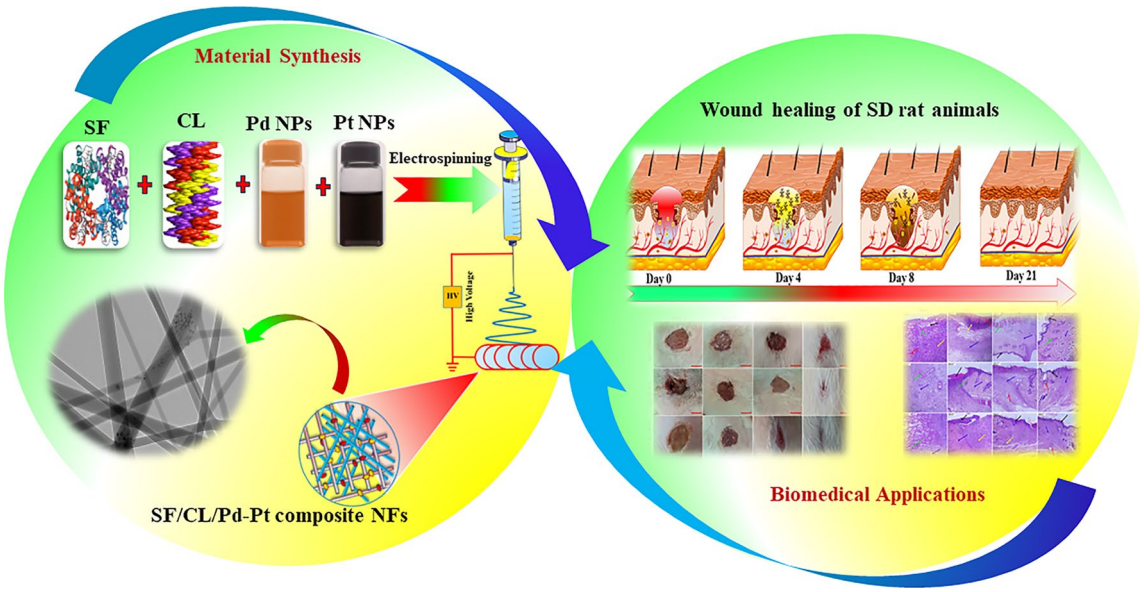

Keywords Nanofiber · Antibacterial · Hemocompatibility · Tissue regeneration · Wound dressing

Introduction

Wound healing is an essential physiological process, crucial for repairing damaged tissues and restoring the integrity of the skin post-injury or surgery. The structural disparity between gram-positive bacteria, typified by *Staphylococcus aureus* (*S. aureus*), with a thick peptidoglycan layer in their cell wall, and gram-negative bacteria like *Escherichia coli* (*E. coli*), characterized by a thinner peptidoglycan layer surrounded by an outer membrane, holds pivotal significance across scientific disciplines, particularly microbiology, and medicine [1]. The innovative strategy for enhancing this intricate process involves leveraging nanofiber matrices, proven to be effective in wound dressing applications. This holistic exploration of wound healing emphasizes the multifaceted role of nanofiber technology in both expediting tissue regeneration and providing a robust defense against bacterial challenges [2]. This dual functionality significantly contributes to the overall success of the wound-healing process. Its significance lies in its ability to prevent infection, foster tissue regeneration, and restore normal functioning to the affected area. The utilization of nanofiber matrices plays a pivotal role in wound healing, proving instrumental in minimizing complications and alleviating pain [3]. In the realm of wound dressing applications, nanofiber scaffolds take center stage due to their exceptional efficacy in promoting rapid granulation and tissue regeneration [4]. The porous structure and expansive surface area of nanofiber scaffolds closely mimic the extracellular matrix (ECM), creating an ideal environment that facilitates cell interactions and expedites the healing process [5]. Furthermore, electrospun nanofibrous scaffolds serve as effective delivery systems for therapeutic agents, concurrently combating bacterial infections at the wound site. Beyond wound dressing, nanofiber matrices find extensive applications in tissue engineering, catering to various tissues such as keratinocytes, fibroblasts, endothelial, and blood vessel cells [6, 7]. They also serve as easily absorbed drugs, enhancing biological reactions [8]. Notably, nanofibers, characterized by a high surface area-to-volume ratio, undergo faster degradation than microfibers, primarily through hydrolytic processes. The wound healing process unfolds in four distinct phases: hemostasis, inflammation, proliferation, and remodeling. Hemostasis marks the initial stage, preventing bleeding or removing blood clots while restoring vascular integrity [9, 10]. The inflammatory phase primary objective is to eliminate bacteria and foster new tissue formation [11]. The proliferative phase witnesses the growth of granulation tissue and angiogenesis as inflammatory cells recede. Lastly, the remodeling phase sees the formation of new dermal and epidermal tissue in the wound recovery area. This comprehensive understanding underscores the intricate and dynamic nature of the wound-healing process, wherein nanofiber matrices contribute significantly to each stage.

The biopolymer materials are silk fibroin, gelatin, collagen, and chitosan, utilized in various biomedical fields such as wound dressing, skin tissue engineering, drug delivery, and studies about antibacterial, antimicrobial, and anticancer properties [12, 13]. Notably, silk fibroin (SF) and collagen (CL) stand out as protein-based biopolymers renowned for their exceptional fiber-forming characteristics and heightened interaction with biological processes [14]. The composite scaffolds crafted from silk fibroin and collagen consist of various amino acids, including glycine, sericin, alanine, proline, and hydroxyproline [15]. These amino acids efficiently serve as reducing and stabilizing agents for metal nanoparticles. Silk fibroin is derived from the *bombyxmori* silkworm cocoon, featuring an inner layer of silk fibroin and an outer layer of sericin [16]. Collagen (CL) is obtained by denaturing animal tissues like skin, muscle, and bone [17]. Collagen is available in various forms such as powder, particles, solution, pastes, and gels, sourced from diverse animals including chicken, bovine, fish, and others [18]. Collagen, particularly, proves highly beneficial for biological activities in wound healing studies. Typically, silk fibroin and collagen composite nanofiber scaffolds exhibit a β-sheet triple helical structure formation [19]. Furthermore, the composite matrix of silk fibroin and collagen showcases outstanding biological activities, including biodegradability and biocompatibility without cytotoxicity. It offers enhanced therapeutic attributes, facilitating easy cell adhesion on substrates, exhibiting low antigenicity, optimal oxygen permeability, and possessing unique mechanical strength [20].

Platinum group metals exhibit high efficacy in various biomedical applications, including wound healing, tissue engineering, and drug delivery. These metal nanoparticles possess unique properties that render them suitable for biomedical purposes, given their biocompatibility, antibacterial characteristics, and ability to induce tissue regeneration [21]. Our focus utilizing biodegradable polymers, specifically silk fibroin and collagen, for synthesizing palladium and platinum metal nanoparticles. Silk fibroin and collagen, being protein based biopolymers obtained in amino acids, serve as effective reducing and stabilizing agents in the synthesis of palladium and platinum metal nanoparticles. Palladium (Pd) and platinum (Pt) nanoparticles play a crucial role in wound treatment, stimulating tissue regeneration and contributing significantly to disease detection [22]. Their primary function involves facile interaction with antibodies, DNA, and RNA molecules, targeting specifically. In this context, it is imperative to develop environmentally friendly methods for synthesizing Pt–Pd NPs without the use of hazardous chemicals and enhance their biomedical properties. These nanoparticles exhibit potent antimicrobial properties, effectively eliminating or hindering the growth of a broad spectrum of bacteria, fungi, and other microorganisms [23]. Furthermore, palladium and platinum nanoparticles have excellent anti-inflammatory attributes, aiding in reducing inflammation at the wound site. Additionally, these nanoparticles readily stimulate the processes of cell proliferation and migration. They also contribute to the formation of new blood vessels, supplying oxygen and nutrients to the healing tissue [24]. Consequently, these nanoparticles hold great promise in the biomedical field, particularly in the realm of wound healing.

In this research work, meticulously designed a bimetallic combination of palladium and platinum nanoparticles, integrated with silk fibroin and collagen composite nanofibers using the electrospinning method. To comprehensively assess the fabricated composite nanofibers, we employed various physicochemical characterization techniques, including fourier transform infrared spectroscopy, field emission scanning electron microscopy with energy dispersive spectroscopy, high-resolution transmittance electron microscopy, atomic force microscopy, X-ray photoelectron spectroscopy, thermogravimetric analysis, mechanical strength, swelling ratio, biodegradation properties, porosity, hemocompatibility, and antioxidant activity. Furthermore, in vitro studies evaluated the antibacterial activity of composite nanofiber materials. The results demonstrated outstanding performance against both gram-positive strains (*S. aureus*) and gram-negative bacteria (*E. coli*). The robust antibacterial capability of SF/CL/Pd–Pt composite nanofibrous scaffolds positions them as excellent candidates for wound healing applications in biomedical settings, where combating bacterial infections is crucial for successful tissue regeneration. Simultaneously, we examined the cell proliferation activity using the fibroblast (NIH3T3) cell line. Subsequently, in vivo studies were conducted to assess the wound healing activity in Sprague Dawley rat animals. The assessed capabilities of SF/CL/Pd–Pt composite nanofibers are high efficiency in absorbing exudates from wound surfaces, promoting cell adhesion, and facilitating tissue regeneration. The findings of our research underscore the significant enhancements in wound healing activity achieved within a short period through the fabrication of SF/CL/Pd–Pt composite nanofibers. This comprehensive exploration contributes valuable insights into the multifaceted capabilities of these composite nanofiber scaffolds as advanced materials for biomedical applications.

Experimental Section

Materials

Bombyxmori silkworm cocoons were procured from the Sericulture Department in Pudukkottai, Tamilnadu. Collagen (marine fish Type-I), sodium carbonate, lithium bromide, formic acid, palladium chloride, and chloroplatinic

acid hexahydrate were acquired from SRL Pvt. Ltd. All the chemicals have a high analytical grade purity of ≥ 96%. The phosphate-buffered saline, DPPH, ethanol, and MTT (3-(4,5-dimethylthiazolyl-2)-2,5-diphenyltetrazolium bromide) were of high analytical grade with a purity of ≥ 97.96% and were obtained from Sigma-Aldrich, India. The dialysis membrane referred to as 12 kDa MWCO (Molecular weight cut off), with a thickness of 15 µm, was purchased from Fisher Scientific Pvt. Ltd., India. All the aqueous solutions are prepared using deionized water.

Preparation of Silk Fibroin Solution from Bombyxmori Silkworm Cocoon

The *bombyxmori* silk cocoon was divided into small pieces and boiled for 30 min, and 0.5 M sodium carbonate was added to a string for 3 h. Following that, the silk fibroin thread formed after being thoroughly rinsed in deionized water to dispose of the glue-like sericin. The degummed silk fibroin was dried in a hot air oven for 2 h before being treated with 9.3 M lithium bromide and heated at 80 °C. As a result, the silk fibroin solution was obtained in a light yellow color. The silk fibroin solution used the dialysis membrane. The dialysis process is followed for 3 days, and every 6 hours, one's changes in water. After dialysis, the silk fibroin solution was centrifuged at 6000 rpm for 10 min to remove some impurities, and the silk fibroin solution was kept at 4 °C and used further process.

Preparation of SF/CL/Pd–Pt Composite Solution

Silk fibroin with collagen was dissolved in a 1:1 ratio of 10 mL acetic acid and water. The 1% polyvinyl alcohol was added to the SF/CL composite solution and stirred continuously for 3 h while the solution was heated at 60 °C. The polyvinyl alcohol purpose increases the viscosity of the SF/CL composite solutions. The next step was to gradually add 10 mL of (0.1 M) $PdCl_2$ solution to the SF/CL composite solution. After stirring 3 h, the SF/CL/Pd composite solution obtained color changed to a light brown. Additionally, 10 mL of (0.1 M) $H_2PtCl_6{\cdot}6H_2O$ solution was gradually added to the SF/CL/Pd composite solution over 2 h while heating at 80 °C with a continuous stirrer. In the end, the SF/CL/Pd–Pt composite solution took on a dark reddish-brown color.

Fabrication of SF/CL/Pd–Pt Composite Nanofiber

The fabrication of SF/CL/Pd–Pt composite nanofiber using the electrospinning method. The prepared SF/CL, SF/CL/Pd, SF/CL/Pt, and SF/CL/Pd–Pt composite solutions without precipitation or air bubbles before using the electrospinning instrument. The composite solution was injected into a 10 mL syringe with a 0.7 mm stainless steel needle and a flow rate of 0.7 mL/hour. The syringe pump was positioned 10 cm away from the drum collector. Throughout the electrospinning process, the drum collector rotated at a speed of 1200 rpm, while a high voltage of 18 kV was applied. The aluminum foil thickness of 0.05 mm was placed over the drum collector surface after nanofiber formation, encapsulating the nanofibers between the foil layers. The resulting SF/CL, SF/CL/Pd, SF/CL/Pt, and SF/CL/Pd–Pt composite nanofibers were stored at room temperature for the following characterization. Figure 1 depicts the SF/CL/Pd–Pt composite nanofibers preparation process.

Swelling Study

Phosphate buffer saline (PBS) was used to test composite nanofiber swelling behavior at different times. Initially, the composite nanofiber was uniformly cut into rectangular shapes sized at 1 × 1 cm and submerged in phosphate buffer saline solution. Then, the nanofibers were weighed until saturation of swelling was reached. The calculated swelling percentage is shown in the equation below.

$$\text{Swelling ratio}\% = \left(\frac{N_w - N_d}{N_d}\right) \times 100, \tag{1}$$

where N_w represents the weight of the wet or swollen nanofiber, and N_d represents the weight of the dry nanofiber.

Degradation Analysis

The degradation analysis of composite nanofiber was conducted in Phosphate buffer saline with a pH level of 7.4 and maintained at 37 °C. In brief, composite nanofibers of known dry weights (Wi) were incubated in PBS for the duration of the study on different days. The PBS was refreshed daily. Triplicates of each sample group were tested for statistical purposes. The degradation rate was determined using below the calculation.

$$\text{Degradationate rate} = \left(\frac{W_i - W_f}{W_i}\right) \times 100, \tag{2}$$

where W_i is the initial weight of the nanofiber and W_f is the final weight of the nanofiber.

Porosity Measurement

The liquid displacement method was used to detect the porosity. The nanofibrous scaffolds measured at 1 × 1 cm, were fully immersed in absolute ethanol until reached saturation. The weight of the nanofibrous grafts was recorded both before and after immersion in ethanol. To ensure accuracy,

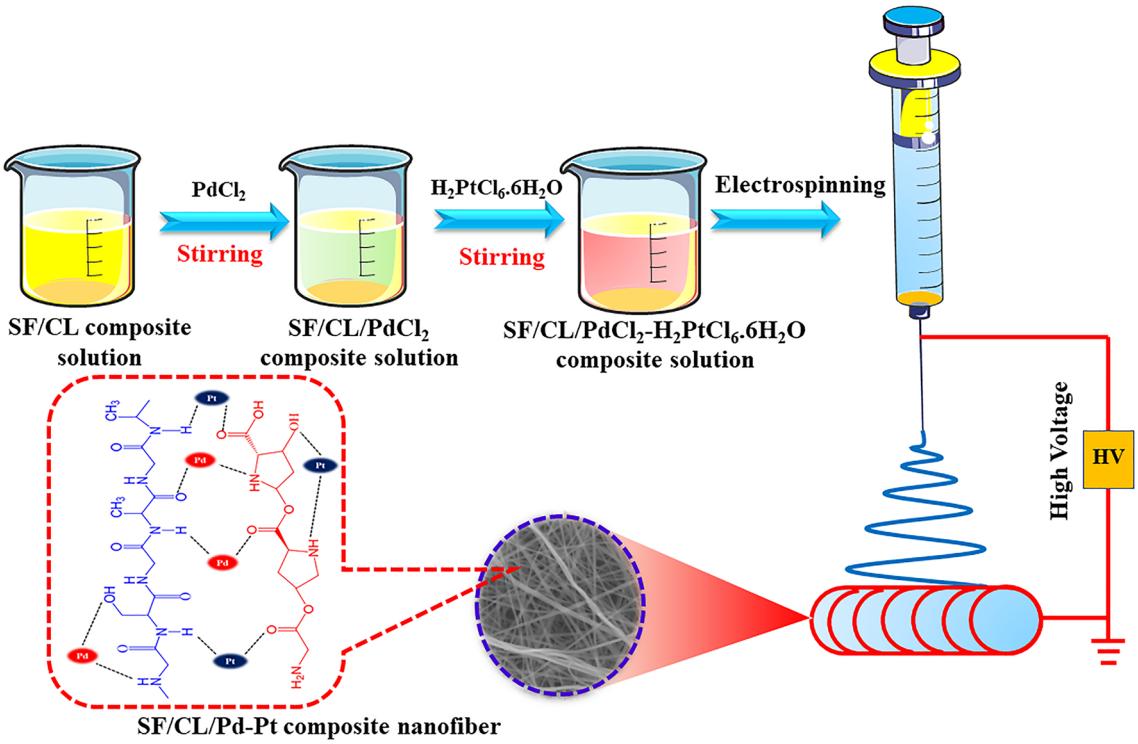

Fig. 1 Schematic representation diagram of the preparation of SF/CL/Pd–Pt composite nanofibers

all samples were measured in triplicate. The porosity was calculated using the following equation.

$$\text{Porosity } \% = \left(\frac{W_3 - W_1}{W_3 - W_2}\right) \times 100, \tag{3}$$

where W_1 is the weight of the dry nanofiber, W_2 is the weight of the nanofiber saturated with ethanol, W_3 is the weight of the nanofiber after removing from ethanol.

Hemocompatibility Test

Examined the hemocompatibility test using blood samples taken from Sprague Dawley rat animals because it is an essential measurement to evaluate the safety of biological materials. The obtained blood sample underwent centrifugation at 1500 rpm for 3 min, resulting in the separation of a pellet while discarding the plasma. The pellet was washed with a standard saline solution through centrifugation at 1500 rpm for 5 min. After removing the supernatant, the Sprague Dawley red blood cells (RBCs) were diluted using a normal saline solution. The SF/CL/Pd–Pt composite nanofiber was cut into equal 1 × 1 cm sizes, added to the RBC, and incubated at 37 °C for 30 min. Subsequently, the RBCs underwent centrifugation at 1500 rpm for 3 min at intervals of 1, 2, 3, and 4 h. The absorption of oxyhemoglobin at 540 nm was measured using a UV–Vis spectrometer. The hemolysis % was calculated below the formula

$$\text{Haemolysis}(\%) = \left[\frac{OD_{test}}{OD_{pos}} - \frac{OD_{neg}}{OD_{neg}}\right] \times 100 \tag{4}$$

Optical density$_{\text{Test}}$ = absorbance measurement of test solution containing nanofiber.

Optical density$_{\text{Negative}}$ = absorbance of negative control,

Optical density$_{\text{Positive}}$ = absorbance of positive control.

Antioxidant Evaluation by DPPH Radical Assay

Initially, DPPH was dissolved in 95% methanol solution and using a phosphate buffer solution with a pH of 6.6 medium and ascorbic acid 10 mg/100 mL. Next, 0.5 mL of fresh DPPH methanol solution was added to the test samples at various concentrations. The absorbance of the DPPH methanol solution was then measured at 517 nm. The discoloration of the test samples indicated their scavenging potential.

$$\text{DPPH scavenging activity } (\%) = \frac{A_0 - A_1}{A_0} \times 100 \tag{5}$$

A_0 = absorbance of control,

A_1 = absorbance of test sample (nanofiber).

In Vitro Assessment of Antibacterial Activity

The disc diffusion method was analyzed to assess the antibacterial activity of the composite nanofibers. As references, two bacterial strains were utilized: the gram-positive *S. aureus* (ATCC33591) and the gram-negative *E. coli* (ATCC10536) were used in the antibacterial assays. The bacterial strains were evenly spread on nutrient agar plates using a glass L-rod, and 100 mL of growing culture was applied under aseptic conditions. Each plate was coated with a 30 mm square and then incubated at 37 °C for 24 h. The zone of inhibition was measured and reported in millimeters (mm) following the incubation period. The concentration at which the growth of the relevant microorganisms was halted was identified as the minimum inhibitory concentration (MIC). The tests were conducted in triplicate.

Cell Proliferation of Fibroblast NIH3T3 Cell Line

Cell proliferation of the fabricated composite nanofibers was evaluated by using the MTT assay. The composite nanofibers underwent treatment with 100% ethanol and UV exposure, followed by washing with deionized water and sterilization for 30 min. After the removal of ethanol, the composite nanofiber matrix was rinsed with PBS and subsequently exposed to a DMEM medium enriched with 10% FBS for 12 h. Fibroblast cells (NIH3T3) were cultured in a medium containing 10% FBS under conditions of 37 °C, 5% CO_2, and 95% humidity. Subsequently, these cells were seeded into 96-well plates, each containing a population of 1×10^4 cells. Following the treatment, each well received 5 mg/mL of MTT suspension and was incubated at 37 °C in a humid environment for 4 h.

$$\text{Cell viability } \% = \left(\frac{\text{Absorbance of Treated Cells}}{\text{Absorbance of Control cells}}\right) \times 100 \tag{6}$$

Methodology of Wound Healing

Animal Acquisition

Two to 3 month old, 180–220 g Sprague Dawley rats were purchased from Mass Biotech in Chengalpattu and transmitted to the pharmacology department animal house. K. K. College of Pharmacy, Chennai, conducted the animal experimentation study. The rats were housed in light to medium-dark conditions with humidity and temperature control, fed a standard pellet diet, and had free access to clean water. The guidelines of the Institutional Animal Ethics Committee (IAEC-KKCP/2021/01/) have been approved by the Committee for the Purpose of Control and Supervision on Experimental Animals (CPCSEA).

In Vivo Wound Healing Assay

The wound healing activity of composite nanofiber scaffolds was evaluated using Sprague–Dawley rat animals. The dorsal area of the rat was shaved using an electronic trimmer, and after the wound was marked, isoflurane anaesthesia was given to the rats. The Sprague–Dawley rat was anesthetized with an intraperitoneal injection of xylazine before a wound was created on its dorsal surface. A round shaped wound size of 1.5×1.5 cm in length and width was created on the rat's dorsal side using a surgical blade and pointer scissors. Each group consisted of four rats, and injured tissue was embedded in paraffin after being fixed in 10% buffered formaldehyde. Afterward, a dressing made of composite nanofiber scaffolds was applied to the rat's dorsal surface area and covered with medical gauze. The composite nanofiber scaffolds were used as the dressing material for the positive control, while medical gauze was used as the negative control. The wound dressings were changed every other day for the 1st week. They were replaced once every 3 weeks for the following 3 weeks. On the fourth, eighth, and 21st days of this period, rats were killed using a lethal dose of thiopental urethane, and on the first, fourth, eighth, and 21st days, photographs of the rat's healed wound were taken with a camera. On the eighth and 21st days, anaesthesia was administered to one chosen rat to evaluate the effects of the 4th day treatment and examine the damaged skin tissue. The remaining rats were given the same treatments for the remaining days. The size of the traced wound area was measured using macroscopical analysis. The percentage of wound healing was calculated using the formula below.

$$\text{Wound healing}\% = \frac{\text{Initial wound size} - \text{Specific day wound size}}{\text{Initial wound size}} \times 100 \tag{7}$$

Staining Analysis

On the specified days, tissue samples from the excisional wounds were gathered for histopathological examination. After being immersed in 10% formalin for 3 days, the tissue sample was treated with formalin-fixed paraffin-embedded tissue blocks of 5 mm thickness and examined using hematoxylin and eosin with Masson trichrome staining. Depending on the various days wound healing was changed. Day 0 represents no healing, Day 4th represents minimal healing (less than 50%), Day 8th represents

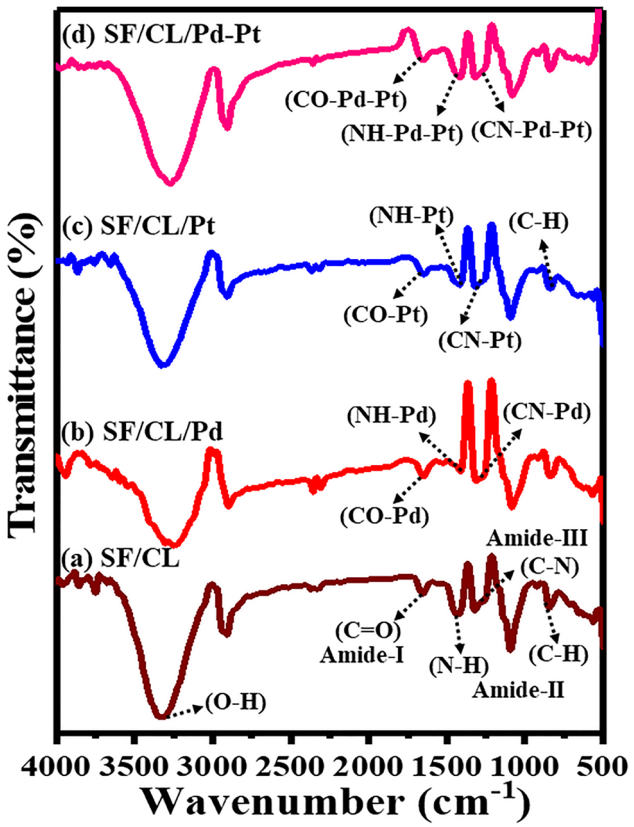

Fig. 2 FTIR spectra of **a** SF/CL, **b** SF/CL/Pd, **c** SF/CL/Pt, and **d** SF/CL/Pd–Pt composite nanofibers

moderate healing (equal to or greater than 50%), and Day 21st represents complete healing.

Skin Irritation Test

Skin sensitization was used to evaluate skin irritation, defined as "reversible damage to the skin." The development of erythema and edoema around wounds on rats covered in nanofiber mat using the Draize test.

Statistical Analysis

The statistical analysis was conducted using a two-way analysis of variance (ANOVA) followed by post hoc Tukey multiple comparison tests, utilizing GraphPad Prism software. Statistical significance levels were determined as single asterisks represent $P < 0.05$, double asterisks represent $P < 0.01$, and quadruple asterisks represent $P < 0.000$.

Results and Discussion

Functional Group Analysis

Fourier transform infrared (FTIR) spectroscopy was used to analyze the functional groups and bonding vibration of the composite materials. The FTIR spectrum of Fig. 2a depicts the silk fibroin and collagen (SF/CL) composite nanofiber matrix as strong absorption intermolecular and intramolecular hydrogen bonds presented in the hydroxy group (O–H) at 3309 cm^{-1} for stretching vibration, the polypeptide (–CONH–)n compound of absorption peaks for amide I, amide II, and amide III amino acids in the silk fibroin and collagen composite matrix [25]. The amide I peak for the carbonyl group was observed in (C=O) stretching vibration at 1651 cm^{-1}, the amide II peak was observed in (N–H) bending vibration at 1557 cm^{-1}, the amide III peak was observed in (C-N) stretching vibration at 1252 cm^{-1}, and the last alkane group was observed in (C–H) stretching vibration at 831 cm^{-1} respectively [26]. The FTIR spectrum of Fig. 2b, c depicts the silk fibroin blended collagen with palladium (SF/CL/Pd) and platinum (SF/CL/Pt) nanoparticle hybrid the composite nanofibre matrix was quickly bonding interaction of carbonyl compound with amide group because this nanofiber matrix was more number of amino acids presented, it hence quickly reacts with a metal nanoparticle interacted to CO-Pd, NH-Pd, and CN-Pd stretching vibration of peak observed at 1645 cm^{-1}, 1509 cm^{-1},1263 cm^{-1}, and CO-Pt, NH-Pt, CN-Pt nanoparticle peaks obtained at 1659 cm^{-1},1526 cm^{-1},1258 cm^{-1} respectively [27]. The FTIR spectrum of Fig. 2d depicts the silk fibroin and collagen incorporated with the palladium and platinum (SF/CL/Pd–Pt) metal nanoparticle hybrid in the composite nanofibre scaffolds as stretching vibrations of the metal–metal bond that interacted with carbonyl compounds and amino groups such as C=O, N–H, and C–N (Pd–Pt) presented at 1682 cm^{-1}, 1507 cm^{-1}, and 1287 cm^{-1}, respectively.

Surface Morphology and Elemental Composition Analysis

Field emission scanning electron microscopy (FESEM) images were used to measure the average diameter size and distinguish the surface morphologies of the composite nanofiber. The image probe tool was more beneficial for measuring the average diameter. The silk fibroin and collagen composite nanofiber (SF/CL) matrix SEM images were well-aligned without beadles and had smooth surface morphology [28], as shown in Fig. 3a, b. The SEM images of Fig. 3c, d show the silk fibroin and collagen blended with palladium nanoparticle composite nanofiber (SF/CL/Pd), were beads formation of cord shape morphology. The

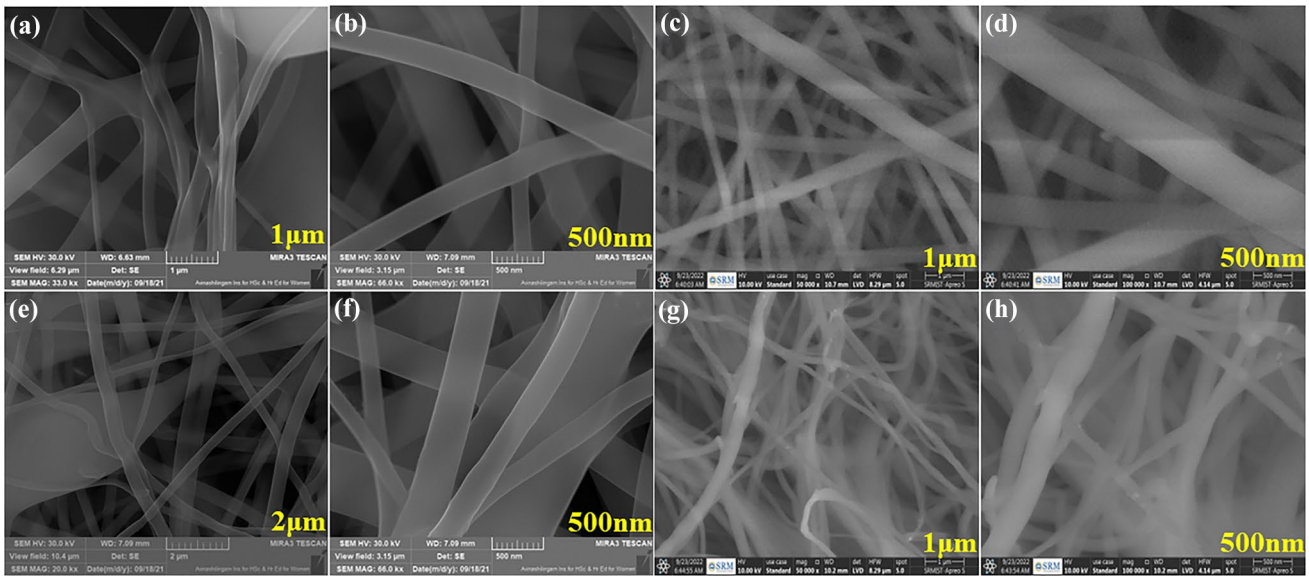

Fig. 3 FE-SEM images of **a, b** SF/CL, **c, d** SF/CL/Pd, **e, f** SF/CL/Pt, and **g, h** SF/CL/Pd–Pt composite nanofibers

SEM images of Fig. 3e, f show the silk fibroin and collagen with platinum nanoparticle composite nanofiber (SF/CL/Pt) with a smooth surface layer and flattened network that formed ripen shape morphology [29]. The SEM images of silk fibroin and collagen combined with the palladium and platinum nanoparticle hybrid composite nanofiber (SF/CL/Pd–Pt) scaffolds with rope-shaped morphology are depicted in Fig. 3g, h. Besides, all the SEM images were measured with different magnifications, such as 2 µm, 1 µm, and 500 nm. The diameter decreases since palladium and platinum metal nanoparticles are strongly clustered in the silk fibroin and collagen composite nanofiber matrix. The nanofiber size distribution histogram images of (Supp. Figure 1) (a) SF/CL composite nanofiber average diameter is 218.12 ± 209.43 nm, (b) SF/CL/Pd composite nanofiber average diameter is 210.76 ± 191.32 nm, (c) SF/CL/Pt composite nanofiber average diameter is 196.93 ± 168.09 nm, and (d) The of the SF/CL/Pd–Pt composite nanofiber average diameter is 178.79 ± 147.08 nm. A smaller diameter size main advantage is higher surface charge density, which can promote cell adhesion and proliferation. The smaller diameter nanofibers are more flexible and can more closely mimic the natural structure of many tissues, improving their biocompatibility and effectiveness as tissue scaffolds [30, 31]. To identify the elemental analysis of the SF/CL/Pd–Pt composite, nanofiber was utilized in energy dispersive X-ray (EDX) spectroscopy. The EDX color mapping images of (Supp. Figure 2) represent the elemental composition of the SF/CL/Pd–Pt composite nanofiber results showed that carbon is red, nitrogen is blue, oxygen is yellow, palladium is violet, and platinum is green. The results of the EDX spectrum indicate that the palladium and platinum nanoparticles are firmly attached to the silk fibroin matrix and collagen composite nanofiber.

Transmittance Electron Microscopy

The composite nanofiber inner layer structure, metal nanoparticle size, and surface morphology were examined using high-resolution transmittance electron microscopy (HR-TEM). The TEM images were measured at different magnifications (100 nm, 50 nm, and 20 nm). TEM images of silk fibroin and collagen (SF/CL) composite nanofibers with single rod morphology [32, 33] are shown in Fig. 4a–c. The TEM images of silk fibroin and collagen with palladium nanoparticles (SF/CL/Pd) composite nanofiber scaffolds were multi-stick linked to the rod shape morphology and visibly detected the palladium metal nanoparticle size at 8.64 nm are shown in Fig. 4d–f. The TEM images of silk fibroin and collagen that anchor the platinum nanoparticles (SF/CL/Pt) composite nanofiber scaffolds were networks with a rod shaped morphology and detected the platinum metal nanoparticle size at 7.36 nm, as depicted in Fig. 4g–i. The TEM images of silk fibroin and collagen anchored in the palladium and platinum nanoparticles (SF/CL/Pd–Pt) composite nanofiber scaffolds were stuck with rod shaped morphology and measured the average diameter size at 141.62 ± 33.03 nm, as depicted in Fig. 4j–l. The TEM images were most helpful in detecting the nanofiber morphology and distinguished metal nanoparticle size.

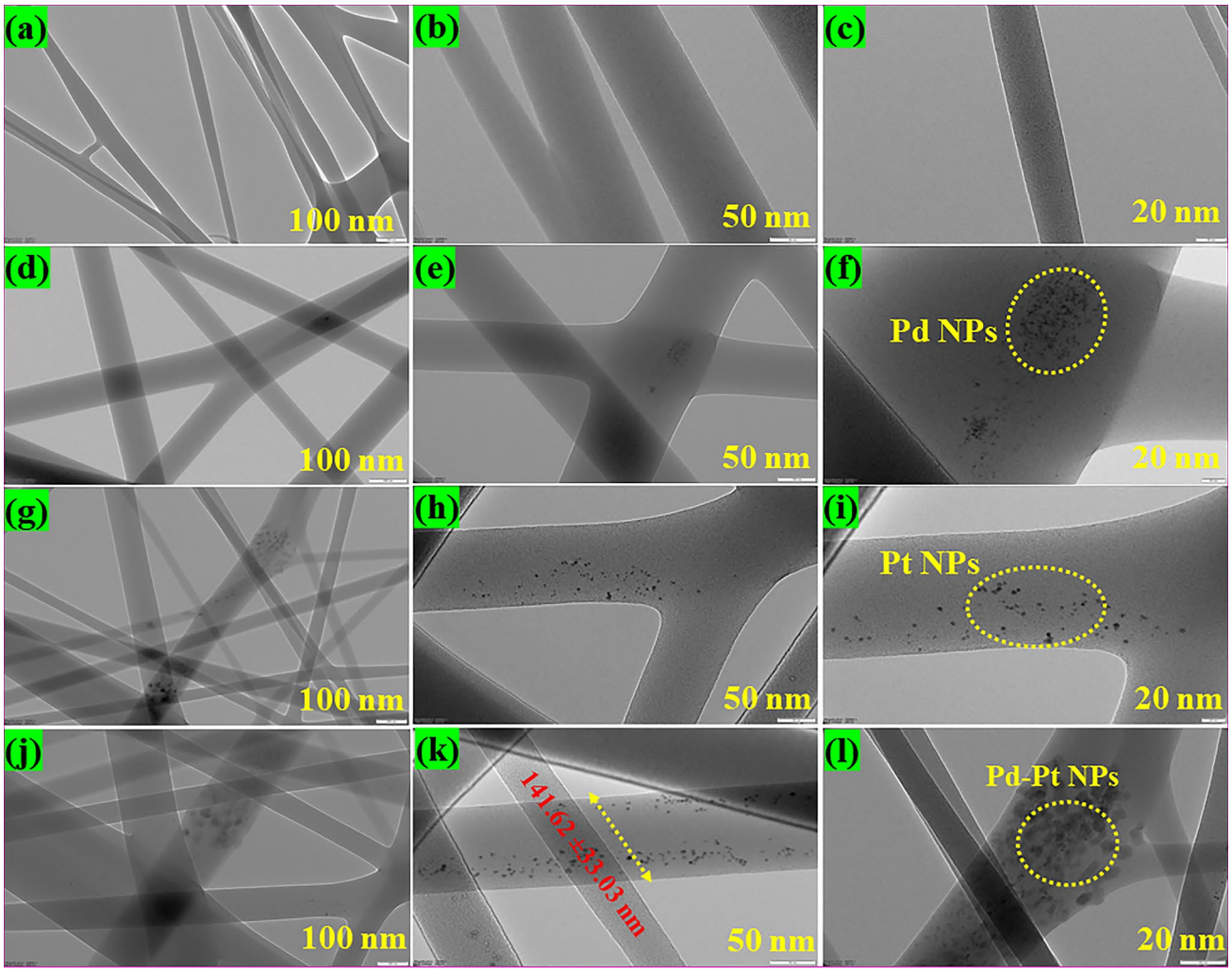

Fig. 4 HR-TEM images of **a–c** SF/CL, **d–f** SF/CL/Pd, **g–i** SF/CL/Pt, and **j–l** SF/CL/Pd–Pt composite nanofiber measured with different magnification (100 nm, 50 nm, and 20 nm)

Nanofiber Thickness and Roughness Analysis

Atomic force microscopy (AFM) is the most advanced technique for determining the structure of two-dimensional and three-dimensional surface morphology. The AFM image was beneficial for detecting the thickness and smoothness of the composite nanofiber scaffolds. The SF/CL, SF/CL/Pd, SF/CL/Pt, and SF/CL/Pd–Pt composite nanofiber matrix for the two-dimensional smoothness structure of rope shape morphology is demonstrated by the AFM pictures of Fig. 5a–d. The topographical image scan rate was approximately measured at 25 µm × 25 µm. The palladium and platinum metal nanoparticles that strongly interact with silk fibroin and collagen composite nanofiber scaffolds are visible in the AFM image, as indicated by the light whitish-brown color. The three-dimensional surface morphology of the SF/CL, SF/CL/Pd, SF/CL/Pt, and SF/CL/Pd–Pt composite nanofiber matrix was measured at 1.71 m, 1.79 m, 1.94 m, and 1.98 m, respectively, according to the AFM images in Fig. 5a–i to d–i. Furthermore, the three-dimensional structure of composite nanofiber surface roughness area (Ra) was determined to be 128.76 nm, 224.56 nm, 294.02 nm, and 312.97 nm, respectively. The roughness area increases the reason of palladium and platinum metal nanoparticles are strongly clustered in the silk fibroin and collagen composite nanofibrous matrix. The composite nanofiber surface roughness area gradually increases the significance for biomedical fields because they have more porosity behavior, making it easier to encourage cell attachment and proliferation to improve the healing adhesion to tissue regeneration [34–36].

Binding Energy Analysis

X-ray photoelectron spectroscopy (XPS) was used to analyze the surface studies of metal oxidation states, binding energy, electronic configuration, and elemental identification of the

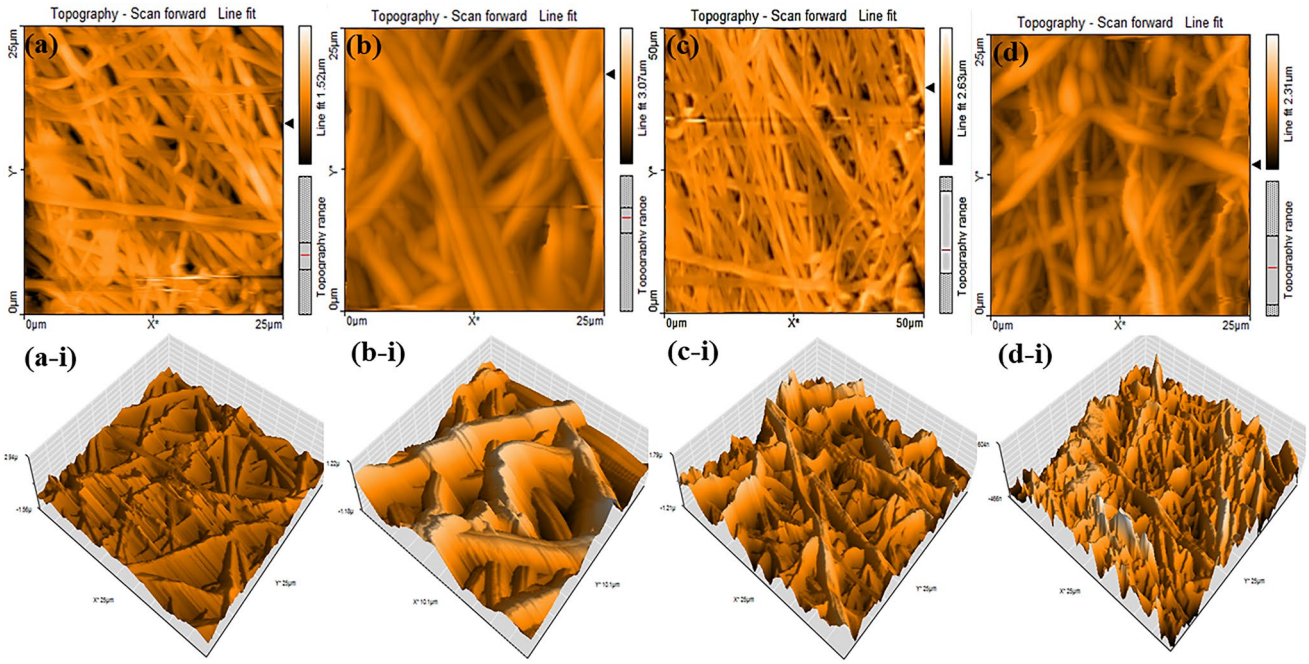

Fig. 5 AFM 2D images of **a**, **b**, **c**, & **d**) SF/CL, SF/CL/Pd, SF/CL/Pt, and SF/CL/Pd–Pt composite nanofiber, and 3D images of (**a–i**, **b–i**, **c–i** & **d–i**) SF/CL, SF/CL/Pd, SF/CL/Pt, and SF/CL/Pd–Pt composite nanofiber

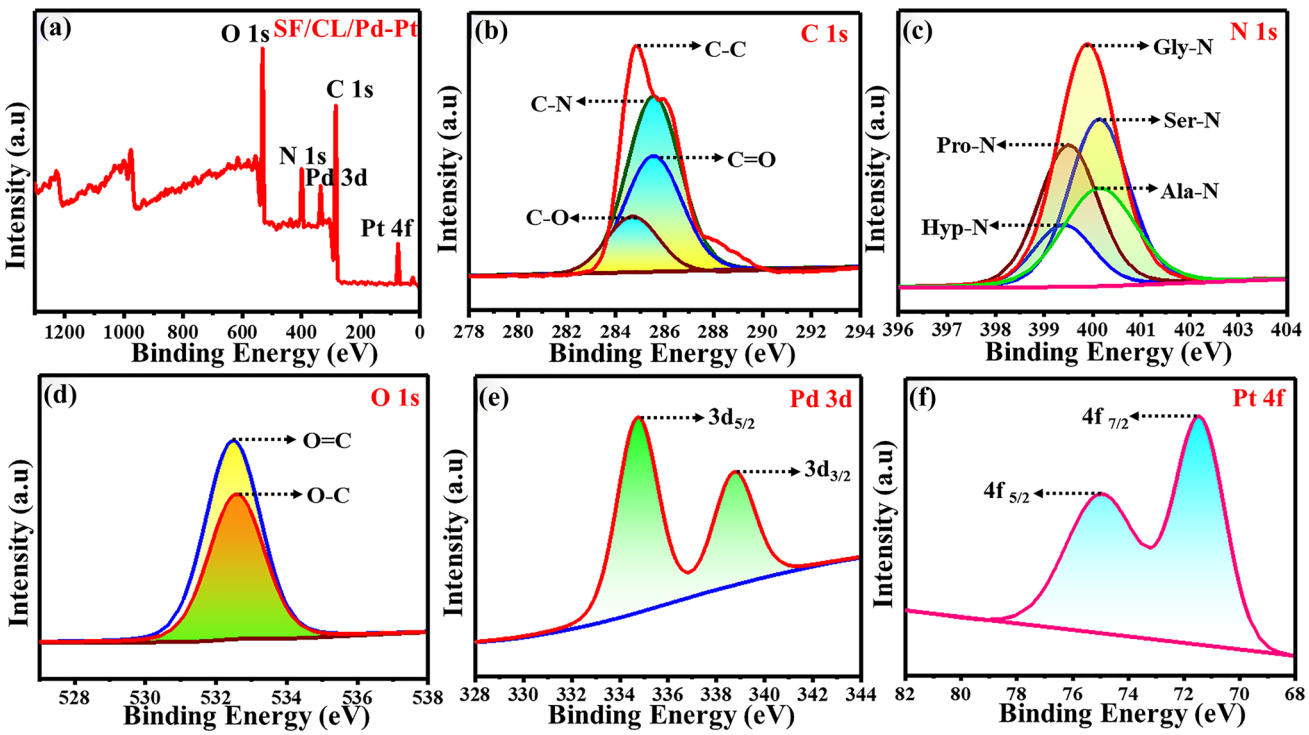

Fig. 6 XPS survey spectrum of **a** SF/CL/Pd–Pt composite nanofiber and corresponding high-resolution XPS survey spectrum of **b** C 1s, **c** N 1s, **d** O 1s, **e** Pd 3d, and **f** Pt 4f

composite nanofiber scaffolds. The overall XPS survey spectrum was depicted in Fig. 6a analysis in SF/CL/Pd–Pt composite nanofiber scaffolds peak intensity indicated that C1s, N1s, O1s, Pd3d, and Pt4f elements were observed the binding energies (eV) were carbon at 285.13 eV, nitrogen at 399.92 eV, oxygen at 532.11 eV, palladium at 366.28 eV, and platinum at 75.05 eV respectively. The full-width half-maximum differentiation of atomic percentages of all elements was predictable in carbon at 67.69%, nitrogen at 13.39%, oxygen at 15.34%, palladium at 2.03%, and platinum at 1.55%. The high-resolution XPS spectrum was C1s split into four distinct peaks for C–C, C–N, C=O, and C–O group of carbon atom overlaps with sp^2 and sp^3 hybridization; these peaks are observed with different binding energies for 284.87 eV, 285.42 eV, 286.63 eV, and 285.23 eV [37] are depicted in Fig. 6b. The high-resolution XPS spectrum was N1s predictable for the nitrogen group of amino acids that have appeared in five different peaks, as well as Glycine, Serine, Alanine, Proline, and Hydroxyproline. The binding energy of Glycine at 399.92 eV, Serine at 400.12 eV, Alanine at 400.02 eV, Proline at 399.42 eV, and Hydroxyproline at 399.33 eV [38] are depicted in Fig. 6c. The high-resolution XPS spectra revealed O1s splitting into two peaks, indicated in carbonyl groups such as O–C and O=C, observed in the silk fibroin and collagen composite matrix. The binding energy of the oxygen atom connected with the carbon atom is 531.94 eV [39], and 532.78 eV is depicted in Fig. 6d. The high-resolution XPS spectrum of Pd3d splitting two different intensity peaks revealed that the binding energies of $Pd3d_{3/2}$ and $Pd3d_{5/2}$ were 338.81 eV and 334.80 eV [40], as shown in Fig. 6e. The chemical oxidation state of Pd nanoparticles is Pd^0 and Pd^{2+}, corresponding with $Pd3d_{3/2}$ and $Pd3d_{5/2}$. The high-resolution XPS spectrum of Pt4f split into two peaks, $Pt4f_{5/2}$ and $Pt4f_{7/2,}$ with binding energies at 75.13 eV and 71.45 eV [41], are depicted in Fig. 6f. The chemical oxidation states of Pt nanoparticles are represented by Pt^0 and Pt^{4+}. The XPS spectra revealed the integration of palladium and platinum nanoparticles into the silk fibroin matrix and collagen composite nanofiber matrix.

Thermal Stability Analysis

The thermal stability and decomposition behaviour of composite nanofibrous scaffolds were examined using thermogravimetric analysis (TGA). The composite nanofibrous was loaded in platinum crucible plates and heated from 20–800 °C for nitrogen gas, passing inert atmospheric conditions at a flow rate of 10 °C/minute. The TGA graph of (Supp. Figure 3) (a) shows the thermal degradation of silk fibroin and collagen (SF/CL) composite nanofiber matrix was weight loss in different temperatures, the first decomposition temperature 225 °C for the elimination of water molecules [42] and removal of some impurity compound. The second, third, and fourth decomposition temperatures are 330 to 525 °C for degrading amino acid and peptide bond cleavages [43, 44]. The TGA graph of (Supp. Figure 3) (b to d) shows the thermal degradation of silk fibroin and collagen loaded with palladium and platinum metal nanoparticles composite nanofiber scaffolds where weight losses were observed at different temperatures (SF/CL/Pd for 260 °C, 375 °C, 457 °C, and 549 °C), (SF/CL/Pt for 265 °C, 387 °C, 485 °C, and 567 °C), and (SF/CL/Pd–Pt for 269 °C, 390 °C, 491°and 578 °C), respectively. The weight loss temperature was slightly different, but the thermal curve was nearly identical in the degradation of silk fibroin and collagen composite nanofibers. Moreover, above the TGA results was the decomposition temperature curve represented by palladium and platinum metal nanoparticles, which are highly incorporated in the silk fibroin and collagen composite matrix. Consequently, the TGA result-wise SF/CL/Pd–Pt composite nanofiber matrix has higher thermal stability than other nanofibrous scaffolds. Additionally, Dynamic Light Scattering (DLS), and mechanical strength of composite nanofiber discussed the Support Figs. 4 and 5.

Swelling and Degradation Analysis

The swelling properties are the most crucial function for controlling cell adhesion, infiltration, and nutrition transfer formation. Figure 7a illustrates the swelling percentage of SF/CL, SF/CL/Pd, SF/CL/Pt, and SF/CL/Pd–Pt composite nanofibers measurement on different days. The SF provides structural integrity and biocompatibility, while CL offers antimicrobial properties and promotes cell adhesion and proliferation. Due to the Pd and Pt metal nanoparticles being firmly incorporated into the SF/CL composite nanofiber due to a highly absorbed hydrophilic group of composite nanofiber scaffolds, the swelling was steady for about 2 days. It started to decrease in the remaining days. Figure 7b depicts the degradation percentages of the SF/CL, SF/CL/Pd, SF/CL/Pt, and SF/CL/Pd–Pt composite nanofibers, which exhibit a high degradation rate at each time point. The SF/CL and SF/CL/Pd–Pt composite nanofiber degradation occurs on various days. The produced SF/CL/Pd–Pt composite nanofiber functions as a diffusion barrier to hydrogen bonds that form between the silk fibroin and collagen matrix, slowing the degradation rate by forming a crosslinking structure. Besides, the swelling and degradation results for SF/CL and SF/CL/Pd–Pt composite nanofibers are excellent, making them well-suited for biomedical applications.

Porosity and Hemocompatibility Analysis

The porosity of nanofiber plays a crucial role in wound healing applications because it facilitates the diffusion of oxygen and nutrients and provides a surface for cell

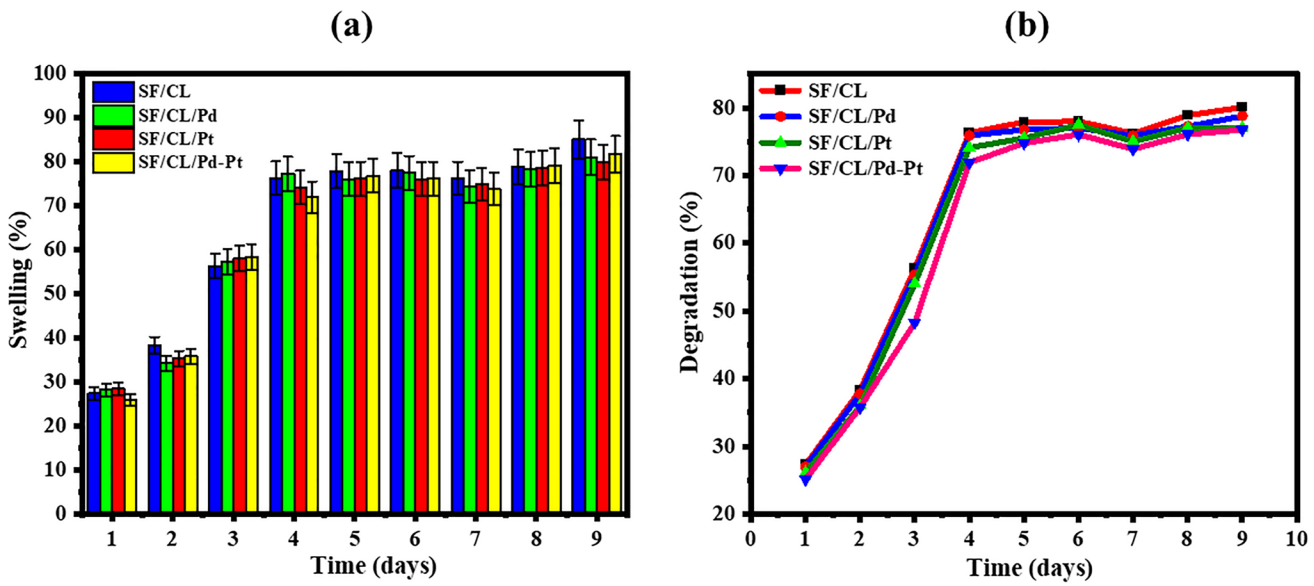

Fig. 7 **a** Swelling and **b** Degradation of SF/CL, SF/CL/Pd, SF/CL/Pt, and SF/CL/Pd–Pt composite nanofiber

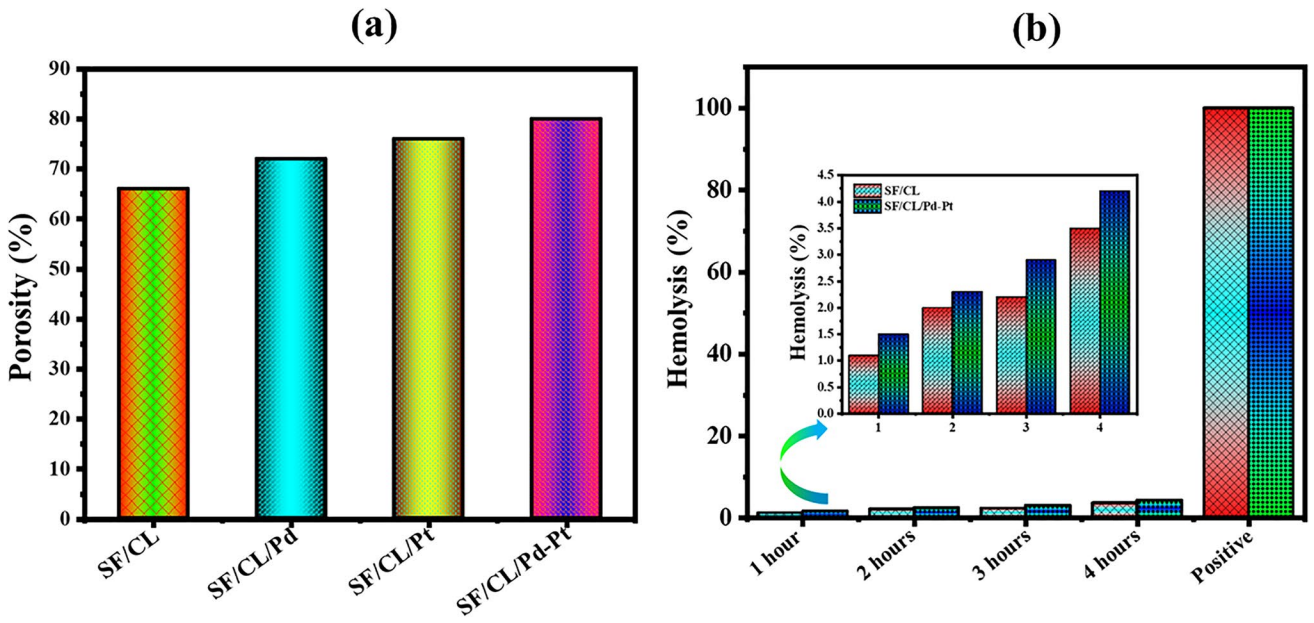

Fig. 8 **a** Porosity of SF/CL, SF/CL/Pd, SF/CL/Pt, and SF/CL/Pd–Pt composite nanofiber. **b** Hemocompatibility of SF/CL and SF/CL/Pd–Pt composite nanofiber

adhesion. The liquid displacement method was used to evaluate the nanofiber scaffolds. Figure 8a indicated the consistent porosity percentages across all nanofiber grafts: 66% for SF/CL, 72% for SF/CL/Pd, 76% for SF/CL/Pt, and 80% for SF/CL/Pd–Pt, even after encapsulating Pd and Pt nanoparticles highly porous nature of the grafts proves advantageous in absorbing exudates from the wound surfaces, making them potentially valuable in developing bioactive implants for pharmaceutical applications in wound healing [45]. The hemolysis assay measures the extent of red blood cell lysis in Sprague Dawley rats at different times. The hemocompatibility study demonstrates that the red blood cell lysis percentage remains below 5%. In particular, the hemocompatibility analysis of the SF/CL/Pd–Pt nanofiber, depicted in Fig. 8b reveals minimal erythrocyte lysis compared to the SF/CL composite nanofiber. Incorporating Pd and Pt nanoparticles into the polymer reduces bioaccumulation. It minimizes contact with the

blood, resulting in erythrocyte lysis percentages of 1.1, 2.0, 2.2%, and 3.5% for the SF/CL composite nanofiber. The SF/CL/Pd–Pt composite nanofiber exhibits erythrocyte lysis percentages of 1.5, 2.3, 2.9, and 4.2%. Therefore, the SF/CL/Pd–Pt nanofiber demonstrates the highest level of hemocompatibility compared to the SF/CL matrix.

Antioxidant Activity of Nanofiber

The antioxidant activity of two different composite matrices, SF/CL and SF/CL/Pd–Pt composite nanofibers were evaluated using the DPPH radical assay method. In the biomedical field, antioxidants are crucial in protecting mutated cells from damage caused by harmful free radicals, which pose risks to human health. The free radical scavenging activity of SF/CL and SF/CL/Pd–Pt composite nanofibers was compared to vitamin C to assess their effectiveness in combating free radicals. The antioxidant activity of Supp. Fig. 6 depicts the composite nanofiber treated with different concentrations such as 10, 20, 50, 75, and 100 µg/mL. The SF/CL composite nanofiber matrix displayed free radical scavenging percentages of 29.36%, 41.35%, 54.84%, 76.19%, and 89.99%. For the SF/CL/Pd composite nanofiber matrix, the percentages were 30.05%, 43.06%, 57.36%, 77.23%, and 90.32%. Similarly, the SF/CL/Pt composite nanofiber matrix exhibited percentages of 31.45%, 44.45%, 60.21%, 778.63%, and 91.09%. As for the SF/CL/Pd–Pt composite nanofibers, their free radical scavenging percentages were 33.69%, 49.56%, 66.02%, 80.23%, and 94.34%. In comparison, the control with vitamin C demonstrated percentages of 20.23%, 31.45%, 49.03%, 61.12%, and 82.33%. The antioxidant activity of SF/CL/Pd–Pt composite nanofibers demonstrated a more substantial effect on the SF/CL composite nanofiber matrix compared with control vitamin C. The palladium and platinum nanoparticles have received much attention in recent years because they have inherent redox characteristics that enable them to participate in reversible redox processes and prevention of oxidative stress-induced damage. In contrast, Pd and Pt nanoparticles can help reduce oxidative stress, which has been linked to various diseases such as cancer, neurological disorders, and cardiovascular disease, by engaging in these redox processes. Moreover, Pd and Pt nanoparticles have also been shown to affect redox signaling pathways; this set off a chain reaction that promotes the activation of natural antioxidant enzymes, including the superoxide dismutase (SOD) reaction [46]. Furthermore, their nanoscale size facilitates cellular absorption and dispersion, allowing them to reach specific cellular interactions in the wound sites. According to this research, Pd and Pt nanoparticles may directly scavenge free radicals due to their direct scavenging ability and redox properties, making them promising candidates for targeted antioxidant therapy.

In vitro Antibacterial and Cell Proliferation of Fibroblast NIH3T3 Cell Line

The antibacterial activity images of Fig. 9a depict the SF/CL and SF/CL/Pd–Pt composite nanofibers tested against two types of bacteria, *S. aureus* and *E.coli*. Compared to the untreated (control), SF/CL and SF/CL/Pd–Pt composite nanofiber matrix. Notably, the Pd–Pt nanoparticle-infused matrix displayed a more significant antibacterial effect compared to the SF/CL composite matrix. Furthermore, it is essential to note that gram-positive (*S. aureus*) and gram-negative (*E. coli*) bacteria have distinct structural differences, likely contributing to the observed variations in efficacy. Gram-positive bacteria possess a thicker and more robust peptidoglycan coating in their cell wall than gram-negative bacteria, whose cell walls are thinner. This structural contrast renders gram-negative bacteria more resilient against antibacterial treatments. The zone of inhibition values for SF/CL composite nanofiber scaffolds against gram-positive (*S. aureus*) and gram-negative (*E.coli*) bacteria were evaluated in Fig. 9b. According to the findings, the zone of inhibition of the SF/CL composite nanofiber scaffold against gram-positive bacteria measured 14 mm, while the zone of inhibition for gram-negative bacteria was determined to be 15 mm. Additionally, SF/CL/Pd–Pt composite nanofiber scaffolds were tested for their zone of inhibition values against the same bacterial strains. The zone of inhibition was 15 mm for *S.aureus* and 17 mm for *E.coli*. Based on these results, the SF/CL/Pd–Pt composite nanofiber scaffolds' antibacterial activity was higher than the SF/CL composite nanofiber matrix. Furthermore, Pd and Pt nanoparticles enhanced the antimicrobial properties of the nanofiber scaffold, leading to more extensive zones of inhibition against both *S. aureus* and *E. coli* bacteria. The larger the zone of inhibition, the more influential the nanofiber scaffold is in inhibiting bacterial growth. The results indicated the SF/CL/Pd–Pt composite nanofibers are more effective in inhibiting the growth of *S. aureus* and *E. coli* growth compared to the control and SF/CL matrix, which is also a highly effective potential material for biomedical applications. Figure 9c and d, the evaluation of the cell proliferation study using the fibroblast NIH3T3 cell line. The fluorescence microscopic pictures of fibroblast cells treated with various concentrations of the composite nanofiber scaffold. These images captured under the fluorescence light microscope used fibroblast NIH3T3 cells clearly regarding the composite nanofiber scaffold cell morphology and cell proliferation at different concentrations, including 25 µg/mL, 50 µg/mL, and 100 µg/mL. Observing these images can assess the proliferation and viability of the fibroblast cells in response to the SF/CL and SF/CL/Pd–Pt composite nanofiber scaffold. Based on these findings, the appropriate concentration of the composite nanofiber scaffold for boosting fibroblast cell growth and

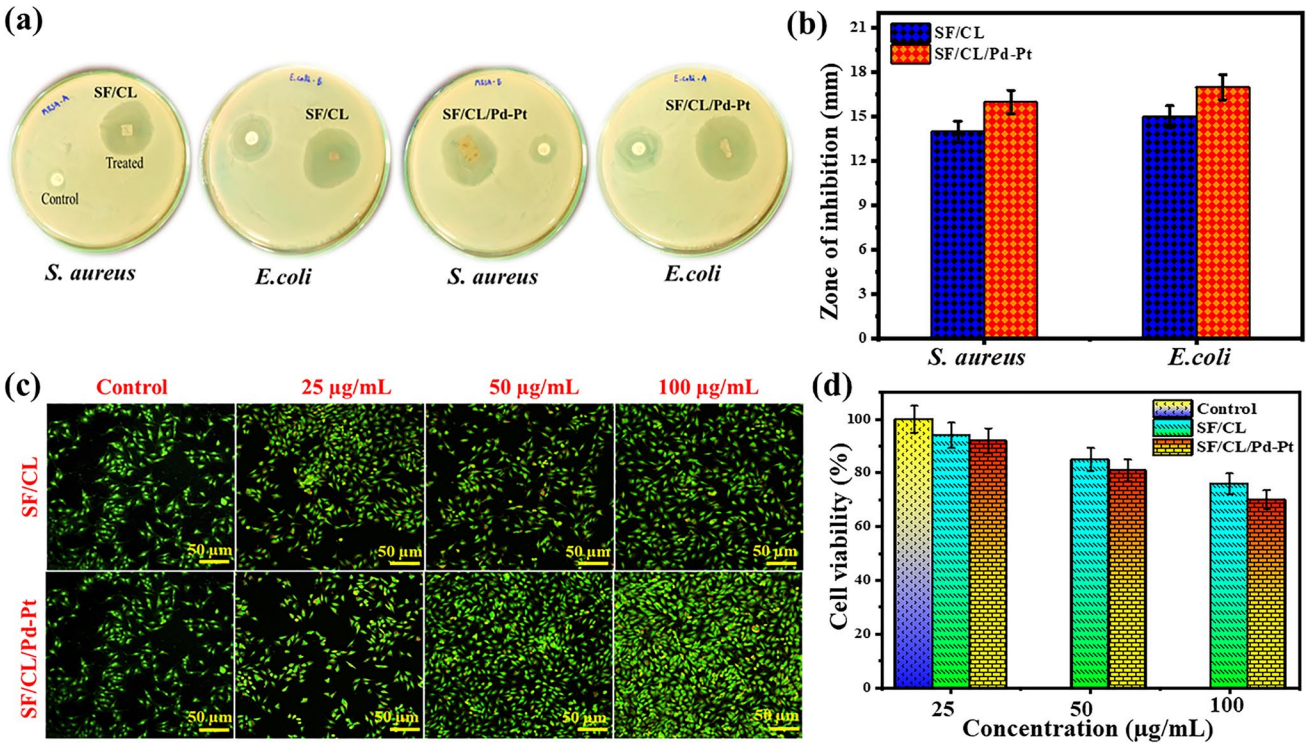

Fig. 9 **a, b** Antibacterial activity images and zone of inhibition of SF/CL and SF/CL/Pd–Pt composite nanofiber using *S.aureus* and *E.coli* staining. **c** Cell proliferation fluorescence microscope images of NIH3T3 fibroblast cell line treated with control, SF/CL, and SF/CL/Pd–Pt composite nanofiber. **d** Cell viability bar representation diagram of SF/CL and SF/CL/Pd–Pt composite nanofiber in different concentrations (25 µg/mL, 50 µg/mL, and 100 µg/mL)

proliferation can be reached. The small size of Pd and Pt nanoparticles is because they possess a larger surface area and carry a positive charge (Pd^+ and Pt^+), which facilitates interaction with negatively charged bacterial membranes. Moreover, the palladium and platinum nanoparticles in silk fibroin and collagen composite nanofiber scaffolds stimulate a cellular response, foster cell development, and enhance biocidal activity. This increased surface area enhances their ability to diffuse through the bacterial wall quickly [47]. In the Supp. Fig. 7 represented the antibacterial activity mechanism of SF/CL/Pd–Pt composite nanofiber interacts with bacterial cell walls, reactive oxygen species, mitochondria damage, and enzyme distribution. In the Supp. Fig. 8 NIH3T3 fibroblast cell seeding images of control, SF/CL, and SF/CL/Pd–Pt composite nanofiber treated with various concentrations such as 25 µg/mL, 50 µg/mL, and 100 µg/mL. Besides, this composite nanofiber material can easily interact with bacterial cells, disrupt the bacterial membrane, and significantly enhance biological activity.

In Vivo Wound Healing Activity of Sprague Dawley Rat Animal

The wound healing performance of a composite nanofiber was evaluated in Sprague Dawley rat animals. The wound healing photographed images in Fig. 10 display the following groups: (a) Control, (b) SF/CL, and (c) SF/CL/Pd–Pt composite nanofibers treated on different days, such as 0th, 4th, 8th, and 21st days. The medical gauze was the negative control, while SF/CL and SF/CL/Pd–Pt composite nanofiber scaffolds were the positive control for wound dressing materials. The (a) control group exhibited a wound healing percentage of 3.10% on the 4th day, 16.00% on the 8th day, and 56.08% on the 21st day, respectively. The wound healing percentage of group (b) silk fibroin and collagen (SF/CL) composite nanofiber matrix was found to be 6.25% on the 4th day, 2.05% on the 8th day, and 78.80% on the 21st day. The wound healing percentage of group (c) silk fibroin/collagen composite nanofiber combined with palladium and platinum nanoparticles (SF/CL/Pd–Pt) was found to be 0% on the 0th day, 15.93% on the 4th day, 41.97% on the 8th day, and 99.63% on the 21st day. After being treated with SF/CL and SF/CL/Pd–Pt composite nanofiber scaffolds, the size of the Sprague–Dawley rat animal wound closure gradually

Fig. 10 Wound healing images of group **a** Control (without treatment), group **b** SF/CL, and group **c** SF/CL/Pd–Pt composite nanofibers treated for 0 day, 4th day, 8th day, and 21st days

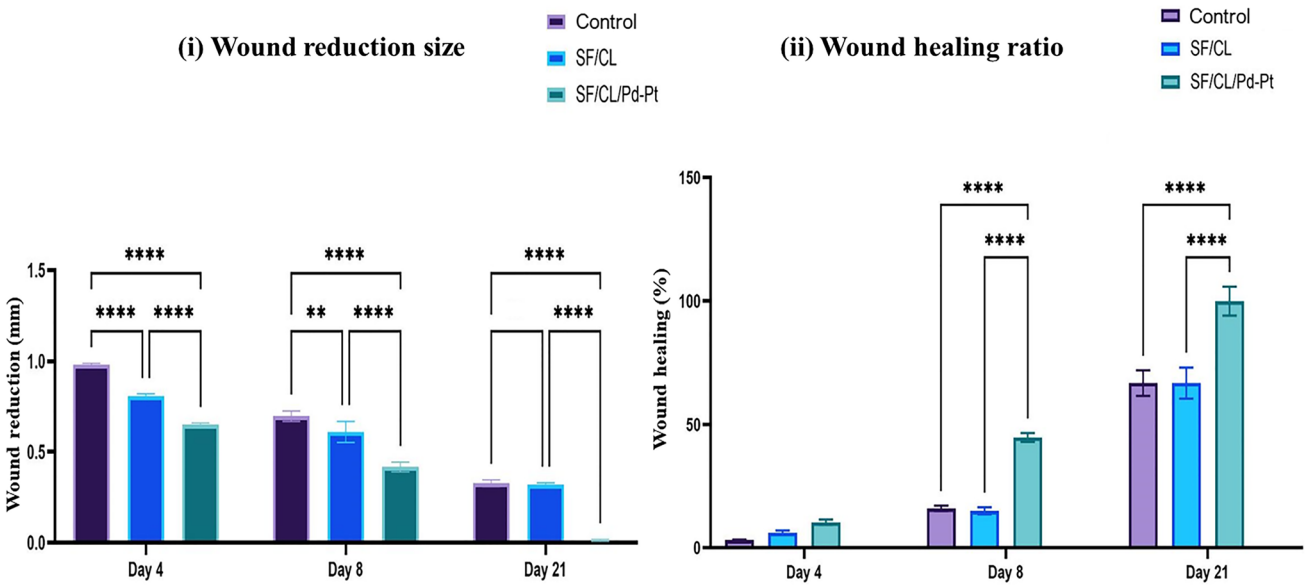

Fig. 11 (i) Wound reduction size and (ii) Wound healing ratio for wound excision in control, SF/CL, and SF/CL/Pd–Pt composite nanofiber for the 4th day, 8th day, and 21st day. The Statistical significance levels were determined as single asterisks represent $P < 0.05$, double asterisks represent $P < 0.01$, and quadruple asterisks represent $P < 0.000$

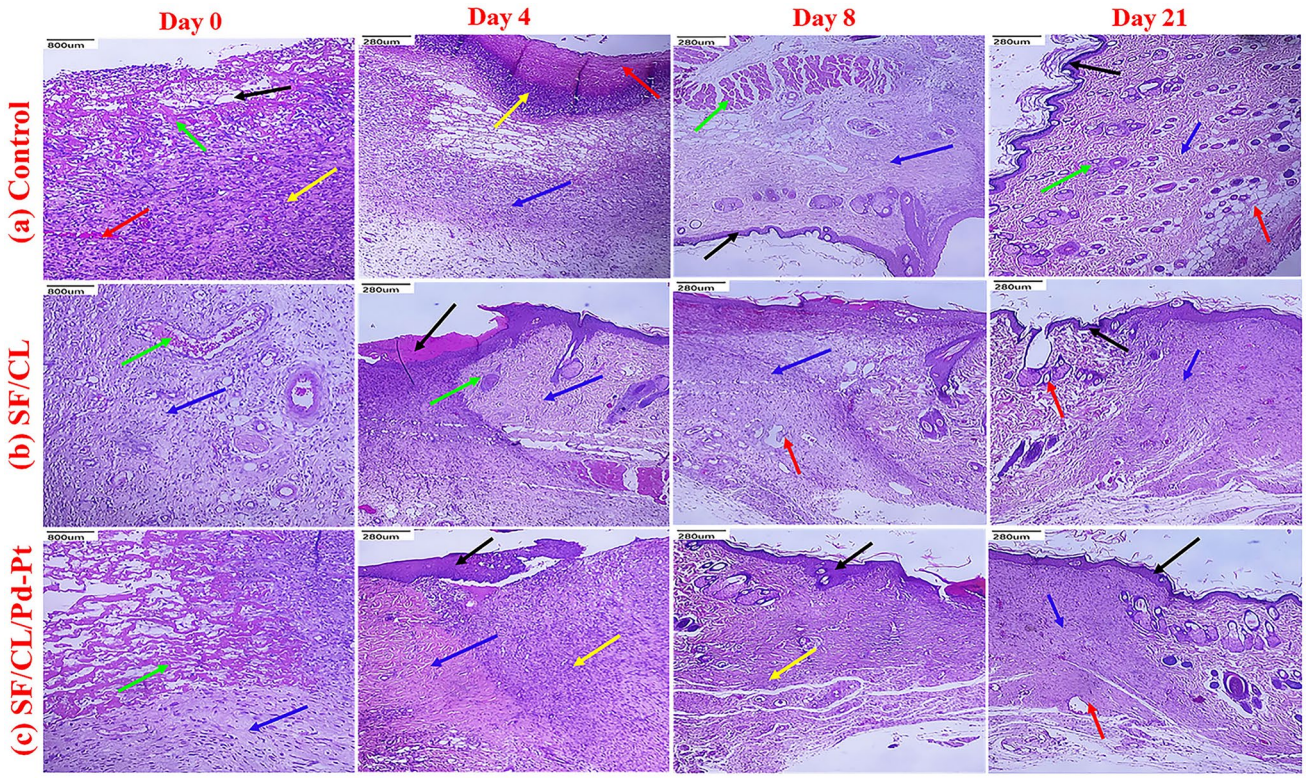

Fig. 12 Histopathological examination of H&E staining images for group **a** Control, group **b** SF/CL, and group **c** SF/CL/Pd–Pt composite nanofibers. Indicated in the images are necrotic debris (black arrow), dense granulation tissue (red arrow), inflammatory cells (yellow arrow), fibroblasts (green arrow), collagen fiber formation (blue arrow), and hair follicles (orange arrow). (Scale bar represents 280 µm) (Color figure online)

shrank. Additionally, SF/CL and SF/CL/Pd–Pt composite nanofibers effectively penetrated the dermal layer, promoting collagen fiber formed at the wound site. The bar diagram representation in Fig. 11 shows the (i) wound reduction size and (ii) wound healing ratio for control, SF/CL, and SF/CL/Pd–Pt composite nanofiber scaffolds. The wound closure size of the Sprague–Dawley rat gradually decreased after treatment with SF/CL and SF/CL/Pd–Pt composite nanofiber scaffolds. As a wound dressing material, silk fibroin with collagen composite nanofibers aids in rat skin regeneration and accelerates wound healing [48]. The Pd and Pt metal nanoparticles can also be powerful anti-angiogenic agents since they are significant therapeutic agents for wound healing [49, 50]. Besides, the final composite of SF/CL/Pd–Pt composite nanofiber mats demonstrated a more favorable healing response with superior epithelialization and wound healing efficiency compared to SF/CL matrix. Also, in vivo study results showed that SF/CL/Pd–Pt composite nanofibers could be used as effective and excellent wound dressing materials, promoting healing by reducing inflammation, removing necrotic cells, and regenerating epithelial cells in wound excision [51].

Hematoxylin and Eosin with Masson Trichrome Staining Analysis

To examine the hematoxylin and eosin staining analysis of the control, SF/CL and SF/CL/Pd–Pt composite nanofiber mats were treated on the 0th, 4th, 8th, and 21st days using Sprague dawley rat animal tissue, as shown in Fig. 12. On the 0 day, the epidermal layer was not obtainable, and there were only a few inflammatory cells formed in all groups, including the control, SF/CL, and SF/CL/Pd–Pt composite nanofiber groups. On the 4th day, we observed epidermal regeneration and the formation of granulation tissue, along with necrotic debris (indicated by black arrow), dense granulation tissue formation (red arrow), inflammatory cells (yellow arrow), fibroblasts (green arrow), and minimal collagen deposition (blue arrow) [52]. On the 8th day, epidermal granulation was obtained, and collagen formed as indicated the (yellow arrow), SF/CL and SF/CL/Pd–Pt composite nanofiber groups effectively absorbed exudates and significantly increased capillary growth in dermal and epidermal tissue formation [53]. Finally, the 21st day observed increased re-epithelialization, more collagen fiber formation (indicated by the blue arrow), intact stratum corneum and

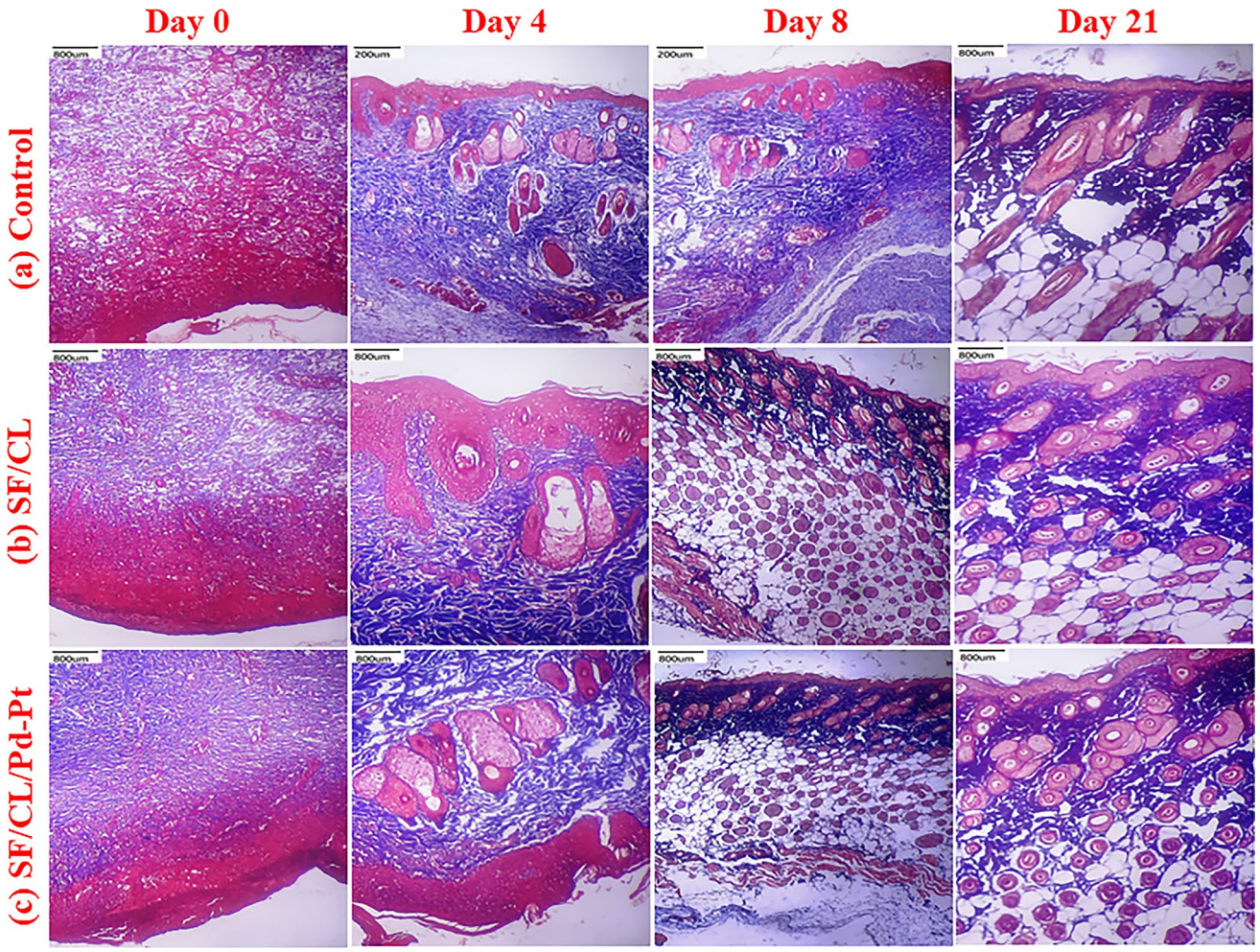

Fig. 13 Histopathological examination of Masson trichrome images of **a** Control, **b** SF/CL, and **c** SF/CL/Pd–Pt composite nanofibers. (Scale bar represents 800 μm)

stratum basalis, and the development of the dermis region and hair follicles (indicated by yellow and orange arrows, respectively) [54].

Masson trichrome staining is a valuable histological technique used to assess collagen deposition and formation in tissue samples. In the context of wound healing studies, it provides crucial insights into the remodeling phase, collagen formation, and deposition play pivotal roles in tissue repair and scar development. Figure 13 shows that Masson trichrome staining was used to detect the tissue regeneration of evaluate three groups: (a) control, (b) SF/CL, and (c) SF/CL/Pd–Pt composite nanofiber scaffolds. In (a) control group serves as a base material for normal wound healing processes without treatment. The staining allows visualization of the natural progression of collagen deposition over time for comparison with the treated groups. In (b) SF/CL nanofiber scaffolds wounds treated with enable the evaluation of the tissue regeneration on collagen formation and deposition, which is indicative of improved wound healing. In (c) SF/CL/Pd–Pt composite nanofiber scaffolds allow for the assessment of more synergistic effects by promoting increased collagen synthesis compared to both the control and SF/CL groups. The synergistic effects of composite nanofiber scaffold have the highest accelerated angiogenesis, leading to improved tissue perfusion and oxygenation. This enhanced vascularization can further support collagen synthesis and deposition, ultimately facilitating faster wound closure and improved tissue regeneration. Then, Pd–Pt nanoparticles could lead to reduced inflammation and minimized scar formation, promoting more favorable wound healing behavior [55, 56]. In all three groups, Masson trichrome staining can provide insights into various aspects of wound healing, including collagen deposition within the wound bed can indicate the efficiency of tissue repair processes. Then, the collagen formation distribution of collagen fibers can reveal the quality of tissue remodeling and scar formation. Overall, Masson trichrome staining provides a robust method for evaluating the tissue regeneration of nanofiber

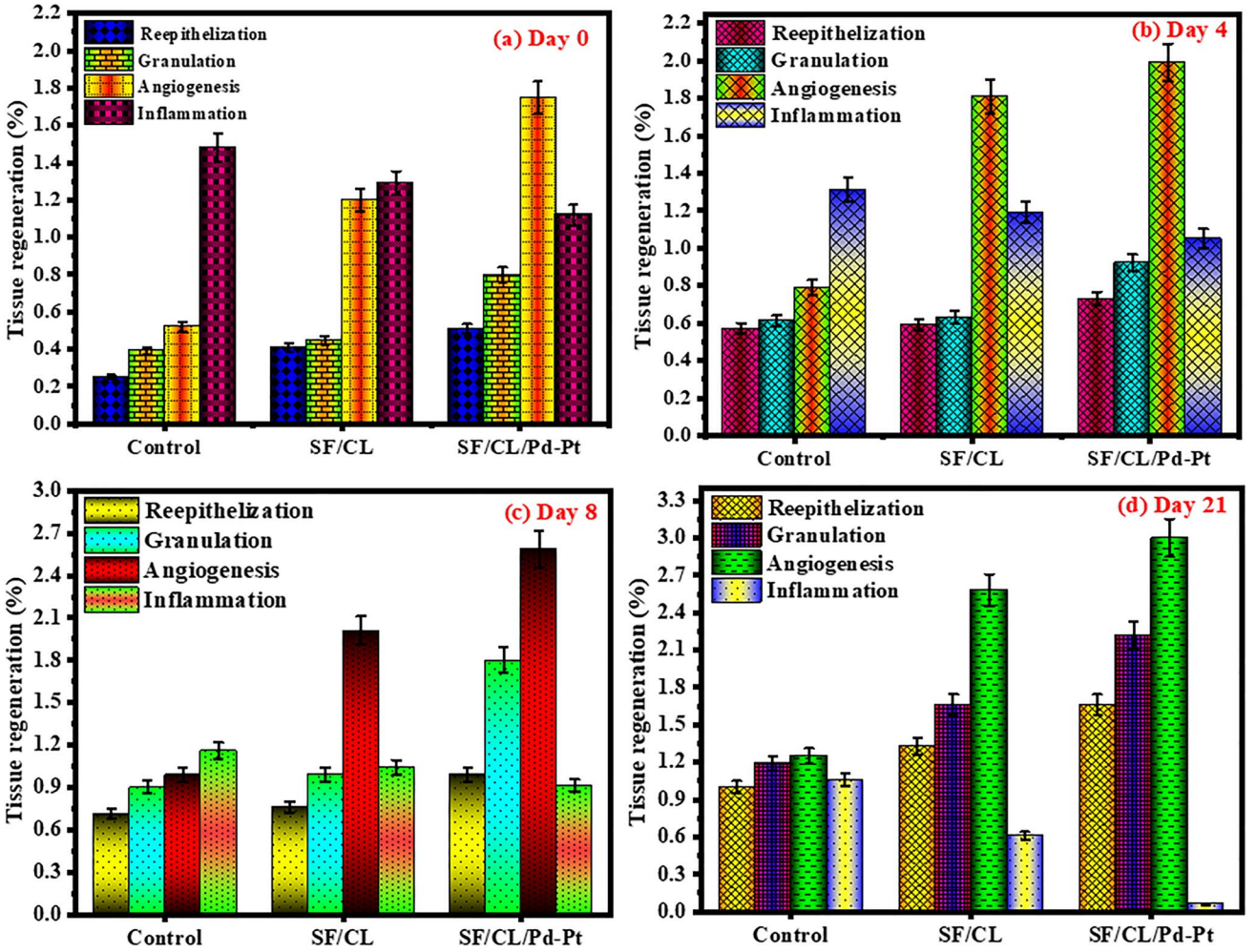

Fig. 14 Tissue regeneration parameters of evaluating the reepithelialization, granulation tissue formation, angiogenesis, and inflammation for control, SF/CL, and SF/CL/Pd–Pt composite nanofiber measured in different days: **a** Day 0, **b** Day 4, **c** Day 8, and **d** Day 21

scaffolds, offering insights into collagen deposition and formation. Through comparative analysis among control and treated groups, the efficiency of SF/CL/Pd–Pt composite nanofiber scaffold material has advanced therapeutic strategies for wound dressing applications.

Figure 14 bar representation diagram of wound excision on different days to evaluate reepithelialization, granulation tissue formation, angiogenesis, and inflammation in three groups: (a) control, (b) SF/CL, and (c) SF/CL/Pd–Pt composite nanofiber scaffolds assess their wound healing activity, specifically focusing on reepithelialization, granulation, angiogenesis, and inflammation. Reepithelialization involves the migration and proliferation of new epithelial cells to cover the wound site and form a new layer of skin [57]. Granulation refers to the formation of new connective tissue and blood vessels, which indicates the ability to support and enhance granulation, facilitating the growth of healthy tissue and promoting the healing process [58]. The angiogenesis is the generation of new blood vessels from pre-existing ones, which is crucial for providing oxygen and nutrients to the wound site. Inflammation is the initial response of the body to an injury or wound involving immune cells, blood vessels, and chemical mediators [59]. The assessment of these SF/CL/Pd–Pt composite nanofiber scaffolds was potential wound healing material was faster reepithelialization, granulation, angiogenesis, and reduced inflammation response.

Conclusion

Successfully designed and fabrication of the SF/CL/Pd–Pt composite nanofiber prepared through the electrospinning method. The nanofiber scaffolds have extraordinary results in terms of antibacterial, and antioxidant activity, improved hemocompatibility, enhanced cell proliferation, and accelerated wound healing capabilities. The notable antibacterial activity of the nanofiber mat can be attributed to various

factors. Silk fibroin and collagen, as constituents, inherently possess antimicrobial properties, inhibiting the growth of diverse bacteria and preventing the colonization of pathogens on wound surfaces. Furthermore, the incorporation of palladium and platinum nanoparticles into the composite plays a crucial role in augmenting antibacterial and antioxidant activities. Extensive research supports the efficacy of these metal nanoparticles in combating a variety of pathogens, potentially causing bacterial cell death and disrupting bacterial cell membranes. The composite nanofiber scaffolds have outstanding wound healing properties are multifaceted. Acting as a scaffold, the nanofibers provide an ideal environment for cellular adhesion, migration, and proliferation, facilitating the regeneration of new tissue and promoting the angiogenesis and reepithelization process. This involves the growth of new blood vessels and the renewal of the skin epidermis. The nanoparticles further stimulate the production of growth factors such as vascular endothelial growth factor (VEGF), essential for angiogenesis and tissue regeneration. This synergistic combination of SF/CL/Pd–Pt composite nanofiber scaffolds position them as excellent biomaterials suitable for a wide range of biomedical applications.

Supplementary Information The online version contains supplementary material available at https://doi.org/10.1007/s10924-024-03261-1.

Acknowledgements The financial support provided to the Rashtriya Uchchatar Shiksha Abhiyan (RUSA-Phase 2.0) Ref. Lr. No. F. 24-51/2014-U, Policy (TNMulti-Gen), Dept. of Education, Government of India

Author Contributions In this manuscript, all persons who meet authorship criteria are listed as authors, and all authors certify that they have participated sufficiently in the work to take public responsibility for the content, including participation in the concept, design, analysis, writing, or revision of the manuscript. Furthermore, each author certifies that this material or similar material has not been and will not be submitted to or published in any other publication before its appearance in the Journal of Polymers and the Environment. Mayakrishnan Arumugam: Conceptualization, Methodology, Investigation; Writing-Original Draft and Formal analysis, Balaji Murugesan: Validation, Resources, Formal analysis, Reviewing and Editing, Dhilipkumar Chinnalagu: Methodology, Formal analysis, Premkumar Balasekar: Resources, Formal analysis and Editing, Yurong Cai: Formal analysis, Reviewing and Editing, Ponnurengam Malliappan Sivakumar: Resources, Formal analysis, Gowri Rengasamy: Methodology, Formal analysis, Krithikapriya Chinniah: Methodology, Formal analysis, Sundrarajan Mahalingam: Validation, Visualization, Supervision.

Funding The financial support provided to the Rashtriya Uchchatar Shiksha Abhiyan (RUSA-Phase 2.0) Ref. Lr. No. F. 24-51/2014-U, Policy (TNMulti-Gen), Dept. of Education, Government of India

Data Availability No datasets were generated or analysed during the current study.

Declarations

Conflict of interest The authors declare no competing interests.

References

1. Zhang Z, Wang J, Luo Y, Li C, Sun Y, Wang K, Deng G, Zhao L, Yuan C, Lu J, Chen Y (2023) A pH-responsive ZC-QPP hydrogel for synergistic antibacterial and antioxidant treatment to enhance wound healing. J Mater Chem B 11(38):9300–9310. https://doi.org/10.1039/D3TB01567J
2. Zahra D, Shokat Z, Ahmad A, Javaid A, Khurshid M, Ashfaq UA, Nashwan AJ (2023) Exploring the recent developments of alginate silk fibroin material for hydrogel wound dressing: a review. Int J Biol Macromol 25:125989. https://doi.org/10.1016/j.ijbiomac.2023.125989
3. Abd Elkodous M, Samuel Oluwaseun O, Sumanta S, Rajesh K (2023) Recent advances in modification of novel carbon-based composites: synthesis, properties, and biotechnological/ biomedical applications. Chem Biol Interact 379:110517. https://doi.org/10.1016/j.cbi.2023.110517
4. Patil PP, Reagan MR, Bohara RA (2020) Silk fibroin and silk-based biomaterial derivatives for ideal wound dressings. Int J Biol Macromol 164:4613–4627. https://doi.org/10.1016/j.ijbiomac.2020.08.041
5. Ghaeli I, De Moraes MA, Beppu MM, Lewandowska K, Sionkowska A, Ferreira-Da-Silva F, Ferraz MP, Monteiro FJ (2017) Phase behaviour and miscibility studies of collagen/silk fibroin macromolecular system in dilute solutions and solid state. Molecules. https://doi.org/10.3390/molecules22081368
6. Zhao G, Zhang Y, Zhang L, Ye ZG, Ren W, Xu F, Wang S, Liu M, Zhang X (2017) 3D conformal modification of electrospun silk nanofibers with nanoscaled ZnO deposition for enhanced photocatalytic activity. ACS Biomater Sci Eng 3:2900–2906. https://doi.org/10.1021/acsbiomaterials.6b00548
7. Martin P, Nunan R (2015) Cellular and molecular mechanisms of repair in acute and chronic wound healing. Br J Dermatol 173:370–378. https://doi.org/10.1111/bjd.13954
8. Heydari P, Zargar Kharazi A, Asgary S, Parham S (2022) Comparing the wound healing effect of a controlled release wound dressing containing curcumin/ciprofloxacin and simvastatin/ciprofloxacin in a rat model: a preclinical study. J Biomed Mater Res A 110:341–352. https://doi.org/10.1002/jbm.a.37292
9. Murugesan B, Arumugam M, Pandiyan N, Veerasingam M, Sonamuthu J, Samayanan S, Mahalingam S (2019) Ornamental morphology of ionic liquid functionalized ternary doped N, P, F and N, B, F-reduced graphene oxide and their prevention activities of bacterial biofilm-associated with orthopedic implantation. Mater Sci Eng C 98:1122–1132. https://doi.org/10.1016/j.msec.2019.01.052
10. Amgarten B, Rajan R, Martínez-Sáez N, Oliveira BL, Albuquerque IS, Brooks RA, Reid DG, Duer MJ, Bernardes GJL (2015) Collagen labelling with an azide-proline chemical reporter in live cells. Chem Commun 51:5250–5252. https://doi.org/10.1039/c4cc07974d
11. Kandhasamy S, Perumal S, Madhan B, Umamaheswari N, Banday JA, Perumal PT, Santhanakrishnan VP (2017) Synthesis and fabrication of collagen-coated ostholamide electrospun nanofiber scaffold for wound healing. ACS Appl Mater Interfaces 9:8556–8568. https://doi.org/10.1021/acsami.6b16488
12. Yaqoob SB, Adnan R, Rameez Khan RM, Rashid M (2020) Gold, silver, and palladium nanoparticles: a chemical tool for biomedical applications. Front Chem 8:1–15. https://doi.org/10.3389/fchem.2020.00376
13. Reizabal A, Brito-Pereira R, Fernandes MM, Castro N, Correia V, Ribeiro C, Costa CM, Perez L, Vilas JL, Lanceros-Méndez S (2020) Silk fibroin magnetoactive nanocomposite films and membranes for dynamic bone tissue engineering strategies. Materialia. https://doi.org/10.1016/j.mtla.2020.100709

14. Siddiqi KS, Husen A (2016) Green synthesis, characterization and uses of palladium/platinum nanoparticles. Nanoscale Res Lett. https://doi.org/10.1186/s11671-016-1695-z
15. Dadras Chomachayi M, Solouk A, Akbari S, Sadeghi D, Mirahmadi F, Mirzadeh H (2018) Electrospun nanofibers comprising of silk fibroin/gelatin for drug delivery applications: thyme essential oil and doxycycline monohydrate release study. J Biomed Mater Res A 106:1092–1103. https://doi.org/10.1002/jbm.a.36303
16. Ghalei S, Nourmohammadi J, Solouk A, Mirzadeh H (2018) Enhanced cellular response elicited by addition of amniotic fluid to alginate hydrogel-electrospun silk fibroin fibers for potential wound dressing application. Colloids Surf B Biointerfaces 172:82–89. https://doi.org/10.1016/j.colsurfb.2018.08.028
17. Ramadass SK, Nazir LS, Thangam R, Perumal RK, Manjubala I, Madhan B, Seetharaman S (2019) Type i collagen peptides and nitric oxide releasing electrospun silk fibroin scaffold: a multifunctional approach for the treatment of ischemic chronic wounds. Colloids Surf B Biointerfaces 175:636–643. https://doi.org/10.1016/j.colsurfb.2018.12.025
18. Ribeiro N, Sousa A, Cunha-Reis C, Oliveira AL, Granja PL, Monteiro FJ, Sousa SR (2021) New prospects in skin regeneration and repair using nanophased hydroxyapatite embedded in collagen nanofibers, nanomedicine nanotechnology. Biol Med 33:102353. https://doi.org/10.1016/j.nano.2020.102353
19. Sun W, Gregory DA, Tomeh MA, Zhao X (2021) Silk fibroin as a functional biomaterial for tissue engineering. Int J Mol Sci 22:1–28. https://doi.org/10.3390/ijms22031499
20. Du C, Li Y, Xia X, Du E, Lin Y, Lian J, Ren C, Li S, Wei W, Qin Y (2021) Identification of a novel collagen-like peptide by high-throughput screening for effective wound-healing therapy. Int J Biol Macromol 173:541–553. https://doi.org/10.1016/j.ijbiomac.2021.01.104
21. Aioub M, Panikkanvalappil SR, El-Sayed MA (2017) Platinum-coated gold nanorods: efficient reactive oxygen scavengers that prevent oxidative damage toward healthy, untreated cells during plasmonic photothermal therapy. ACS Nano 11:579–586. https://doi.org/10.1021/acsnano.6b06651
22. Shibuya S, Ozawa Y, Watanabe K, Izuo N, Toda T, Yokote K, Shimizu T (2014) Palladium and platinum nanoparticles attenuate aging-like skin atrophy via antioxidant activity in mice. PLoS ONE. https://doi.org/10.1371/journal.pone.0109288
23. Czarnomysy R, Radomska D, Szewczyk OK, Roszczenko P, Bielawski K (2021) Platinum and palladium complexes as promising sources for antitumor treatments. Int J Mol Sci. https://doi.org/10.3390/ijms22158271
24. He SB, Yang L, Lin MT (2021) Platinum group element-based nanozymes for biomedical applications: an overview. Biomed Mater. https://doi.org/10.1088/1748-605X/abc90416:32001
25. Yang S, Li X, Liu P, Zhang M, Wang C, Zhang B (2020) Multifunctional chitosan/polycaprolactone nanofiber scaffolds with varied dual-drug release for wound-healing applications. ACS Biomater Sci Eng 6:4666–4676. https://doi.org/10.1021/acsbiomaterials.0c00674
26. Arumugam M, Murugesan B, Malliappan P (2023) Electrospun silk fibroin and gelatin blended nanofibers functionalized with noble metal nanoparticles for enhanced biomedical applications. Process Biochem 124:221–234. https://doi.org/10.1016/j.procbio.2022.11.019
27. Polini A, Pagliara S, Stabile R, Netti GS, Roca L, Prattichizzo C, Gesualdo L, Cingolani R, Pisignano D (2010) Collagen-functionalised electrospun polymer fibers for bioengineering applications. Soft Matter 6:1668–1674. https://doi.org/10.1039/b921932c
28. Wang J, Yang Q, Cheng N, Tao X, Zhang Z, Sun X, Zhang Q (2016) Collagen/silk fibroin composite scaffold incorporated with PLGA microsphere for cartilage repair. Mater Sci Eng C 61:705–711. https://doi.org/10.1016/j.msec.2015.12.097
29. Rho KS, Jeong L, Lee G, Seo BM, Park YJ, Hong SD, Roh S, Cho JJ, Park WH, Min BM (2006) Electrospinning of collagen nanofibers: effects on the behavior of normal human keratinocytes and early-stage wound healing. Biomaterials 27:1452–1461. https://doi.org/10.1016/j.biomaterials.2005.08.004
30. Felicitas P, Sascha B, Nadja S, Goran M, Sabine D, Daniel Dietrich R (2022) Physiological oxygen and co-culture with human fibroblasts facilitate in vivo-like properties in human renal proximal tubular epithelial cells. Chem Biol Interact. https://doi.org/10.1016/j.cbi.2022.109959
31. Balakrishnan SB, Kuppu S, Thambusamy S (2021) Biologically important alumina nanoparticles modified polyvinylpyrrolidone scaffolds in vitro characterizations and it is in vivo wound healing efficacy. J Mol Struct 1246:131195. https://doi.org/10.1016/j.molstruc.2021.131195
32. Balakrishnan SB, Alam M, Ahmad N, Govindasamy M, Kuppu S, Thambusamy S (2021) Electrospinning nanofibrous graft preparation and wound healing studies using ZnO nanoparticles and glucosamine loaded with poly(methyl methacrylate)/polyethylene glycol. New J Chem 45:7987–7998. https://doi.org/10.1039/d0nj05409g
33. Qi P, Zeng J, Tong X, Shi J, Wang Y, Sui K (2021) Bioinspired synthesis of fiber-shaped silk fibroin-ferric oxide nanohybrid for superior elimination of antimonite. J Hazard Mater 403:123909. https://doi.org/10.1016/j.jhazmat.2020.123909
34. Arumugam M, Murugesan B, Pandiyan N, Chinnalagu DK, Rangasamy G, Mahalingam S (2021) Electrospinning cellulose acetate/silk fibroin/Au-Ag hybrid composite nanofiber for enhanced biocidal activity against MCF-7 breast cancer cell. Mater Sci Eng C. https://doi.org/10.1016/j.msec.2021.112019
35. Murugesan B, Pandiyan N, Arumugam M, Sonamuthu J, Samayanan S, Yurong C, JumingS. Y (2020) Mahalingam, fabrication of palladium nanoparticles anchored polypyrrole functionalized reduced graphene oxide nanocomposite for antibiofilm associated orthopedic tissue engineering. Appl Surf Sci. https://doi.org/10.1016/j.apsusc.2020.145403
36. Kasinathan K, Marimuthu K, Murugesan B, Samayanan S, Panchu SJ, Swart HC, Savariroyan SRI (2021) Synthesis of biocompatible chitosan functionalized Ag decorated biocomposite for effective antibacterial and anticancer activity. Int J Biol Macromol 178:270–282. https://doi.org/10.1016/j.ijbiomac.2021.02.127
37. Wang LJ, Zhang J, Zhao X, Xu LL, Lyu ZY, Lai M (2015) Palladium nanoparticles functionalized graphene nanosheets for Li-O 2 batteries : enhanced performance by tailoring the morphology of the discharge product. RCS Adv 5:73451–73456. https://doi.org/10.1021/acs.jpcc.6b10882
38. Chen J, Niu Q, Chen G, Nie J, Ma G (2017) Electrooxidation of methanol on Pt @Ni bimetallic catalyst supported on porous carbon nanofibers. J Phys Chem C 121:1463–1471. https://doi.org/10.1021/acs.jpcc.6b10882
39. Zhang Y, Liu Y, Jiang Z, Wang J, Xu Z, Meng K, Zhao H (2021) Poly(glyceryl sebacate)/silk fibroin small-diameter artificial blood vessels with good elasticity and compliance. Smart Mater Med 2:74–86. https://doi.org/10.1016/j.smaim.2021.01.001
40. Chen ZJ, Shi HH, Zheng L, Zhang H, Cha YY, Ruan HX, Zhang Y, Zhang XC (2021) A new cancellous bone material of silk fibroin/cellulose dual network composite aerogel reinforced by nano-hydroxyapatite filler. Int J Biol Macromol 182:286–297. https://doi.org/10.1016/j.ijbiomac.2021.03.204
41. Zhang D, Li L, Shan Y, Xiong J, Hu Z, Zhang Y, Gao J (2019) In vivo study of silk fibroin/gelatin electrospun nanofiber dressing loaded with astragaloside IV on the effect of promoting wound healing and relieving scar. J Drug Deliv Sci Technol 52:272–281. https://doi.org/10.1016/j.jddst.2019.04.021
42. Wu J, Wang S, Zheng Z, Li J (2022) Fabrication of biologically inspired electrospun collagen/silk fibroin/bioactive glass

composited nanofibrous scaffold to accelerate the treatment efficiency of bone repair. Regen Ther 21:122–138. https://doi.org/10.1016/j.reth.2022.05.006
43. Wang Q, Zhou S, Wang L, You R, Yan S, Zhang Q, Li M (2021) Bioactive silk fibroin scaffold with nanoarchitecture for wound healing. Compos Part B Eng 224:109165. https://doi.org/10.1016/j.compositesb.2021.109165
44. Xiao L, Wu M, Yan F, Xie Y, Liu Z, Huang H, Yang Z, Yao S, Cai L (2021) A radial 3D polycaprolactone nanofiber scaffold modified by biomineralization and silk fibroin coating promote bone regeneration in vivo. Int J Biol Macromol 172:19–29. https://doi.org/10.1016/j.ijbiomac.2021.01.036
45. Wang Y, Zhang M, Yan Z et al (2024) Metal nanoparticle hybrid hydrogels: the state-of-the-art of combining hard and soft materials to promote wound healing. Theranostics 14:1534
46. Desai MP, Patil RV, Pawar KD (2020) Green biogenic approach to optimized biosynthesis of noble metal nanoparticles with potential catalytic, antioxidant and antihaemolytic activities. Process Biochem 98:172–182. https://doi.org/10.1016/j.procbio.2020.08.005
47. Anila PA, Keerthiga B, Ramesh M, Muralisankar T (2021) Synthesis and characterization of palladium nanoparticles by chemical and green methods: a comparative study on hepatic toxicity using zebrafish as an animal model. Comp Biochem Physiol C Toxicol Pharmacol 244:108979. https://doi.org/10.1016/j.cbpc.2021.108979
48. Huang K, Jinzhong Z, Zhu T, Morsi Y, Aldalbahi A, El-Newehy M, Yan X, Mo X (2020) PLCL/Silk fibroin based antibacterial nano wound dressing encapsulating oregano essential oil: fabrication, characterization and biological evaluation. Colloids Surf B Biointerfaces 196:111352. https://doi.org/10.1016/j.colsurfb.2020.111352
49. You C, Li Q, Wang X, Wu P, Ho JK, Jin R, Zhang L, Shao H, Han C (2017) Silver nanoparticle loaded collagen/chitosan scaffolds promote wound healing via regulating fibroblast migration and macrophage activation. Sci Rep 7:1–11. https://doi.org/10.1038/s41598-017-10481-0
50. Murugesan B, Pandiyan N, Kasinathan K, Rajaiah A, Arumuga M, Subramanian P, Sonamuthu J, Samayanan S, Arumugam VR, Marimuthu K, Yurong C, Mahalingam S (2020) Fabrication of heteroatom doped NFP-MWCNT and NFB-MWCNT nanocomposite from imidazolium ionic liquid functionalized MWCNT for antibiofilm and wound healing in Wistar rats: synthesis, characterization, in-vitro and in-vivo studies. Mater Sci Eng C 111:110791. https://doi.org/10.1016/j.msec.2020.110791
51. Peng Y, Ma Y, Bao Y, Liu Z, Chen L, Dai F, Li Z (2021) Electrospun PLGA/SF/artemisinin composite nanofibrous membranes for wound dressing. Int J Biol Macromol 183:68–78. https://doi.org/10.1016/j.ijbiomac.2021.04.021
52. Chouhan D, Chakraborty B, Nandi SK, Mandal BB (2017) Role of non-mulberry silk fibroin in deposition and regulation of extracellular matrix towards accelerated wound healing. Acta Biomater 48:157–174. https://doi.org/10.1016/j.actbio.2016.10.019
53. Sylvester MA, Amini F, Keat TC (2019) Electrospun nanofibers in wound healing. Mater Today Proc 29:1–6. https://doi.org/10.1016/j.matpr.2020.05.686
54. White ES, Mantovani AR (2013) Inflammation, wound repair, and fibrosis: reassessing the spectrum of tissue injury and resolution. J Pathol 229:141–144. https://doi.org/10.1002/path.4126
55. Bloch K, Pardesi K, Satriano C, Ghosh S (2021) Bacteriogenic platinum nanoparticles for application in nanomedicine. Front Chem 9:1–11. https://doi.org/10.3389/fchem.2021.624344
56. Xu X, Zhang J, Wang X (2024) Multifunctional Pd single-atom nanozyme for enhanced cascade chemodynamic therapy of chronic wounds. ACS Appl Nano Mater. https://doi.org/10.1021/acsanm.3c06198
57. Chlumsky O, Purkrtova S, Michova H, Sykorova H, Slepicka P, Fajstavr D, Ulbrich P, Viktorova J, Demnerova K (2021) Antimicrobial properties of palladium and platinum nanoparticles: a new tool for combating food-borne pathogens. Int J Mol Sci. https://doi.org/10.3390/ijms22157892
58. Agarwal Y, Rajinikanth PS, Ranjan S, Tiwari U, Balasubramnaiam J, Pandey P, Arya DK, Anand S, Deepak P (2021) Curcumin loaded polycaprolactone-/polyvinyl alcohol-silk fibroin based electrospun nanofibrous mat for rapid healing of diabetic wound: an in-vitro and in-vivo studies. Int J Biol Macromol 176:376–386. https://doi.org/10.1016/j.ijbiomac.2021.02.025
59. Dhanavel S, Manivannan N, Mathivanan N, Gupta VK, Narayanan V, Stephen A (2018) Preparation and characterization of cross-linked chitosan/palladium nanocomposites for catalytic and antibacterial activity. J Mol Liq 257:32–41. https://doi.org/10.1016/j.molliq.2018.02.076

Publisher's Note Springer Nature remains neutral with regard to jurisdictional claims in published maps and institutional affiliations.

Springer Nature or its licensor (e.g. a society or other partner) holds exclusive rights to this article under a publishing agreement with the author(s) or other rightsholder(s); author self-archiving of the accepted manuscript version of this article is solely governed by the terms of such publishing agreement and applicable law.